The Astronomical Journal, 159:15 (17pp), 2020 January https://doi.org/10.3847/1538-3881/ab5525

Binary Stars in Upper Scorpius

Andrei Tokovinin and Cesar Briceño
Cerro Tololo Inter-American Observatory, Casilla 603, La Serena, Chile; atokovinin@ctio.noao.edu
Received 2019 September 27; revised 2019 November 5; accepted 2019 November 5; published 2019 December 13

Abstract

To address the statistics of binary stars in the 8 Myr old Upper Scorpius (USco) star formation region, we conducted a speckle interferometric survey of 614 association members more massive than 0.4 $\mathcal{M}_\odot$ (spectral types earlier than M3V) based on the list of Luhman et al. (2018). We resolved 187 pairs, 55 of which are new discoveries. Also using the published data and the *Gaia* DR2, a catalog of 250 physical binaries was produced. We carefully estimated detection limits for each target and studied binary statistics in the separation range from 0.″06 to 20″ (9–2800 au), as well as clustering at larger separations. The frequency of companions with mass ratios $q > 0.3$ in this separation range is 0.33 ± 0.04 and 0.35 ± 0.04 for early M- and solar-type stars, respectively, larger by 1.62 ± 0.22 and 1.39 ± 0.18 times compared to field stars of similar masses. The excess is produced mostly by pairs closer than 100 au. At separations from 100 to 10^4 au, the separation distribution and companion fraction resemble those of solar-type stars in the field. However, unlike in the field, we see a relative deficit of equal-mass binaries at separations of ∼500 au, compared to smaller and larger separations. The distribution of q depends on the separation, with a preference of larger q and a larger fraction of twins with $q > 0.95$ at smaller separations. The binary population of USco differs from binaries in the field in several ways and suggests that binary statistics is not universal.

Unified Astronomy Thesaurus concepts: Binary stars (154); Star forming regions (1565); Visual binary stars (1777); Multiple stars (1081)

Supporting material: machine-readable tables

1. Introduction

Several surveys of binary stars in young stellar populations have been conducted since the 1990s. Their main goal has been to document differences in binary statistics as a function of density and age and to compare with binaries in the field. Early findings that the binary frequency in the Taurus–Auriga group is substantially higher than in the field provided a strong stimulus to these surveys. The current status is reviewed by Duchêne & Kraus (2013). Statistics of young binaries contribute to our understanding of binary star formation and, consequently, star formation in general.

A popular explanation of the large multiplicity in low-density environments like Taurus (compared to clusters and the field) invokes dynamical disruption of wide binaries by passing stars. In this paradigm, the binary properties at birth are universal, and this hypothetical primordial binary population is modified by "dynamical processing" in clusters (e.g., Kroupa & Petr-Gotzens 2011). However, pure dynamical evolution does not explain the excess of tight binaries in Taurus–Auriga because those pairs are too "hard" (i.e., close and strongly bound) to be destroyed dynamically (King et al. 2012; Parker & Meyer 2014). Meanwhile, large hydrodynamical simulations of collapsing molecular clouds by Bate (2014) demonstrated that wide binaries cannot form in dense environments, while the binaries that do form are hard enough to survive the *N*-body interactions with their neighbors. The idea of a universal primordial binary population and its dynamical processing is therefore inconsistent with both theory and observations (Duchêne et al. 2018).

Given that the binary formation does depend on the environment, it is of the utmost importance to characterize it observationally in star-forming regions of varying stellar density, metallicity, and age over a large range of masses. However, until very recently, we lacked statistically significant samples of young stars in the solar vicinity spanning a wide range of binary separations, stellar masses, and environments. First and foremost, large, reliable membership samples are needed, and these have been hard to assemble, even for the nearest star-forming regions, which are those most amenable for probing binarity down to small separations. Unfortunately, even then, the small size of the stellar population of some of the closest clusters and associations (e.g., ϵ Cha; Briceño & Tokovinin 2017) precludes detailed statistical inferences. Therefore, our current knowledge is fragmentary and inconclusive (Duchêne & Kraus 2013; Reipurth et al. 2014).

The nearby (∼140 pc) Upper Scorpius (USco) OB association (the denser part of the larger Sco OB2 group) contains an updated list of about 1600 known members (Luhman et al. 2018). The association is highly structured spatially, rather than expanding from a common center; its age is about 8 Myr (Wright & Mamajek 2018; David et al. 2019). It contains the largest stellar population younger than ∼10 Myr within 300 pc, providing a unique opportunity to learn new details of the binary star statistics.

Statistics of binary stars in USco were studied by several groups using high-resolution and seeing-limited imaging. Yet only a fraction of the known association members have been examined so far. Recently, we studied multiperiodic stars in USco discovered by *Kepler K2*, assumed to be binaries (Rebull et al. 2018, hereafter RSC18), and, indeed, we resolved most of them (Tokovinin & Briceño 2018). The majority of those pairs were not known previously owing to the incompleteness of prior surveys. We found an unusually narrow distribution of projected separations, with only a few binaries being wider than 1″. The distribution differs markedly from the solar-type binaries in the field (Raghavan et al. 2010; Tokovinin 2014).

This study convinced us that a new large and uniform binary survey of USco is necessary. The capability of our speckle instrument to observe hundreds of stars per night and the astrometry from *Gaia* (Gaia Collaboration et al. 2018) make the present survey both practical and timely.

The input sample of USco members is defined and characterized in Section 2. New speckle interferometric observations of the complete sample are presented in Section 3. In Section 4 we add data from *Gaia* and other sources and give a comprehensive census of resolved binaries. The binary statistics (distributions of mass ratio and separation and their dependence of mass) are studied in Section 5. The results are discussed and compared to other studies in Section 6.

2. The Sample of USco Stars

A sample of the members of the USco association that is not biased with respect to the binary population is the starting point of our survey. At first glance, the availability of accurate parallaxes and proper motions (PMs) in the *Gaia* DR2 catalog (GDR2; Gaia Collaboration et al. 2018) makes this task easy. However, the GDR2 does not provide astrometry of many resolved binaries with separations from $0\farcs1$ to $\sim1''$. Moreover, the PMs and parallaxes of binary stars in the GDR2 are affected by their orbital motions. Therefore, a sample based on the *Gaia* astrometry would be strongly biased against binaries. Recently, Damiani et al. (2019) used the GDR2 to study the membership of the Sco OB2 association, including USco. Their work gives interesting insights on the spatial and kinematical structure of this region, but it is not a good starting point for binary statistics.

We considered the sample of USco members compiled by RSC18. It is restricted to objects within the *Kepler K2* Campaign 2 field and contains ~1300 stars. The membership criteria used by these authors did not rely on the GDR2 catalog, which had not yet been released at the time of their study. Comparison with the GDR2 reveals that the RSC18 sample of USco has a nonnegligible fraction of nonmembers (about 15%). Moreover, we suspect that binary stars with separations of a few arcseconds and components of comparable brightness, semi-resolved by *Kepler*, have been removed from the sample because they are not suitable for precise photometry.

We constructed a control sample of USco members by selecting all GDR2 sources with parallaxes above 5 mas in the rectangular area with $239^\circ < \alpha < 251^\circ$ and $-30^\circ < \delta < -17^\circ$, filtering on parallax (between 5.5 and 9 mas) and PM (μ^*_α from -15 to -5, μ_δ from -28 to -15 mas yr^{-1}) and keeping stars brighter than $G = 15$ mag. Although the control sample of 664 targets is biased against close binaries and is not used here for binary statistics, it is useful for checking other biases.

For our binary survey, we use the large sample of USco members featured in the papers by Esplin et al. (2018, hereafter E18) and Luhman et al. (2018; hereafter L18)—in short, Luhman's sample. These authors combined the astrometric membership criteria (with a suitable allowance for errors) with photometry and used the youth criteria, such as lithium line, emissions, and IR excess. The highly extincted region near the ρ Oph cluster is explicitly avoided. Table 1 in L18 has 1631 entries. The matching Table 6 in E18 contains 1608 stars. Here we use the latter source, as it duplicates the essential information from L18 and also contains the *K*-band photometry.

Table 1
Filtered Luhman's Sample

Col.	Label	Format	Description, Units
1	USn	I4	Number in E18
2	α	F10.5	R.A. (J2000), deg
3	δ	F10.5	decl. (J2000), deg
4	ϖ	F8.2	Parallax, mas
5	μ^*_α	F8.2	PM in R.A., mas yr^{-1}
6	μ_δ	F8.2	PM in decl., mas yr^{-1}
7	V	F6.2	V magnitude, mag
8	G	F6.2	*Gaia* magnitude, mag
9	$V-K$	F6.2	Color index, mag
10	A_K	F6.2	Extinction from E18, mag
11	M_*	F6.2	Estimated mass, $M_\odot$
12	SF	I2	Secondary component

(This table is available in its entirety in machine-readable form.)

The sample derived from Table 6 of E18 has been cross-matched with GDR2; all sources within a $20''$ radius (2800 au at 140 pc) from each star were retrieved to identify potential binary companions. The radius is chosen to avoid confusion between true binaries and random pairs of association members (see Section 5.3). Only 11 faint stars with $K \sim 15$ mag from Luhman's sample are not found in GDR2; they are probably too faint in the *Gaia G* band. Naturally, we do not discard the 107 stars without parallaxes in GDR2 because they are resolved binaries, as we show below. The *Gaia* photometry allows us to compute the *V*-band magnitude from the *G* magnitude and the color index $C = \mathrm{BP}-\mathrm{RP}$ using the recommended transformation,[1]

$$V \approx G + 0.0176 + 0.00686\ C + 0.1732\ C^2. \quad (1)$$

For the survey, we initially selected 744 stars of spectral type M3V or earlier because the remaining stars are too faint for our instrument (see below). We observed in the *I* filter and therefore estimated the *I* magnitudes from *V* and $V-K$ using an approximate polynomial relation derived by fitting isochrones of normal main-sequence stars,

$$I \approx V - 0.196 + 0.2548\ (V-K) + 0.04567\ (V-K)^2. \quad (2)$$

Stars fainter than $I = 13$ mag were removed from the sample, as well as stars with GDR2 parallaxes less than 5 mas and larger than 15 mas and a high extinction of $A_K > 0.3$ mag. This leaves the filtered sample of 614 stars for our survey. The cutoffs on spectral type and magnitude leave the sample stars more massive than $\sim0.4\ M_\odot$. Ten stars in the sample are secondary companions to other, brighter targets, so the sample consists of 604 stellar systems.

The filtered input sample is presented in Table 1 (the table is available in full electronically; its format is given in the text). In column 12, we assign a "1" to stars that are secondary companions, while primary stars have a "0." The distribution of the stars in the sky in Figure 1 resembles Figure 1 of L18. The distribution of PMs, not plotted here, shows a tight

[1] See Chapter 5.3.7 of the *Gaia* DR2 documentation at https://gea.esac.esa.int/archive/documentation/GDR2/.

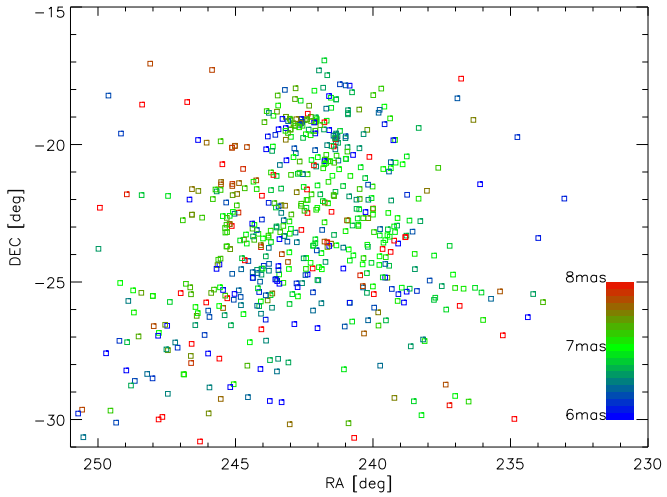

Figure 1. Distribution of the filtered sample on the sky. The nominal limits of Luhman's sample are from 233.°75 to 251.°25 in R.A. and −30° to −16° in decl. The region near ρ Oph is avoided. The symbols are colored by parallax (6 mas in blue, 7 mas in green, 8 mas in red), as shown by the color bar.

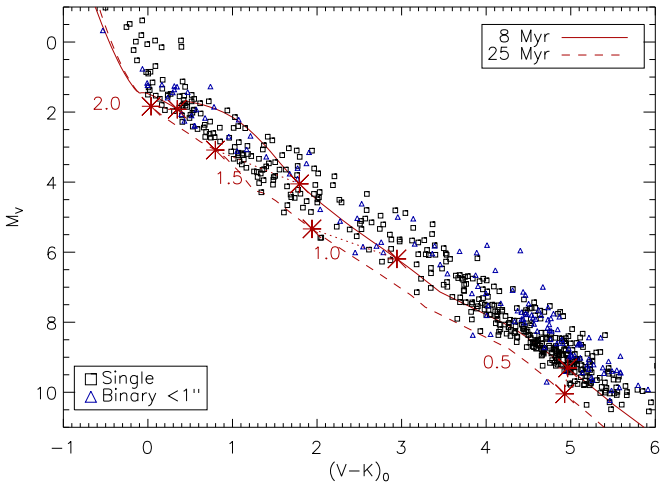

Figure 2. The CMD for the filtered main sample. The solid and dashed lines are the 8 and 25 Myr isochrones (Tang et al. 2014). Large asterisks and numbers mark masses on both isochrones. Individual parallaxes and extinctions are used. Binary stars closer than 1″ are plotted by blue triangles.

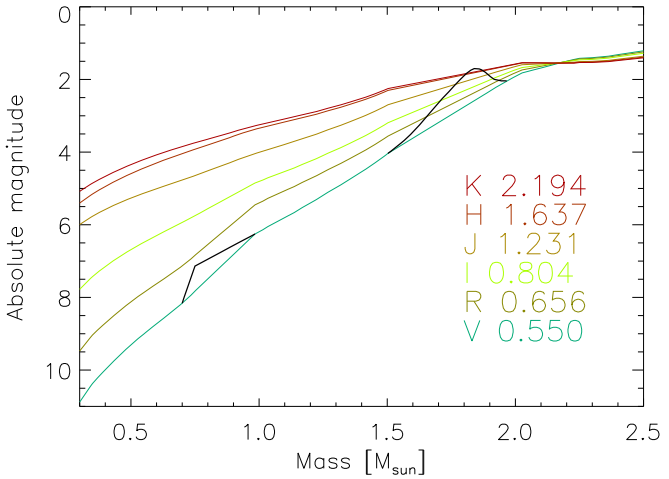

Figure 3. Relation between mass and absolute magnitude in different bands from V to K (bottom to top) according to the PARSEC 8 Myr isochrone for solar metallicity (Tang et al. 2014). Isochrones in the mass intervals [1.5, 1.95] $\mathcal{M}_\odot$ and [0.7, 1.0] $\mathcal{M}_\odot$ were linearly interpolated to avoid the nonmonotonic behavior (the original isochrone in V in these areas is overplotted with black lines).

concentration to the median PM of (−11.20, −23.60) mas yr^{-1}. Luhman et al. used the radius of 10 mas yr^{-1} around the median PM for selecting members of USco but included some PM outliers if their young age was proven by other criteria. We note a positive correlation between μ_α and R.A., apparently reflecting the complex structure of the USco association (Wright & Mamajek 2018; Damiani et al. 2019). The slope is ∼1 mas yr^{-1} per degree of R.A. Its inverse value, sort of an expansion age, is 4 Myr. No other correlations between position and PM are evident. The median parallax is 6.99 mas; 91% of the parallaxes are between 6 and 8 mas.

The filtered sample contains 35 targets without parallaxes and PMs in GDR2. All of those stars, without exception, are resolved binaries. Whenever GDR2 does provide astrometry for a binary, the results might still be inaccurate and/or biased. For example, all four targets with parallaxes larger than 10 mas (US0288, US0690, US0733, and US0745) are binaries, and their parallax errors are large, from 0.4 to 1.3 mas. Selecting an input USco sample based on GDR2 astrometry, like our control sample, inevitably creates a bias against binaries.

The relation between the extinction-corrected $(V-K)_0$ color and the spectral type is almost linear for stars earlier than K0V. This allows us to compute the intrinsic colors and the extinction for these stars from the spectral types provided in L18. The standard extinction law implies $E_{V-K} \approx 8A_K$. However, we found a shallower empirical relation, $E_{V-K} \approx 5A_K$. We do not know whether this discrepancy is caused by the nonstandard (gray) extinction in USco or a bias of the A_K estimates in L18. We apply the extinction corrections using the empirical slope of 5 and obtain a tighter sequence on the color–magnitude diagram (CMD). The CMD of the main sample is shown in Figure 2 (unknown distances are assumed to be 140 pc, parallax 7.1 mas). The overall band is quite thick for several reasons, e.g., binaries, an age spread, or an intrinsic spread in luminosity.

Candidate members of USco from Table 2 of L18 have been evaluated in the same way as the main sample and cross-matched with GDR2. Extinction for these stars was not provided by L18. For the most part, the candidates are low-mass stars, already well represented in the main sample. Many candidates have spectral types later than our limit M3V. For this reason, we do not consider candidate members in our survey and base it only on the filtered main sample.

We estimate the masses of the stars from their absolute magnitudes M_V corrected for extinction using the 8 Myr PARSEC isochrone for solar metallicity (Tang et al. 2014). We prefer the V band because the dependence on mass is steeper than in the K band; hence, errors in M_V (e.g., caused by binary companions) have less influence on the derived masses (Figure 3). In order to get a monotonic relation between M_V and mass, we eliminated the "kink" around 1.8 $\mathcal{M}_\odot$ and the discontinuity around 0.7 $\mathcal{M}_\odot$ by linear interpolation of all isochrones in these two regions (see the black lines in Figure 3). Such patching of the isochrones is necessary for correct evaluation of masses and mass ratios.

Understandably, the masses M_* are only crude and possibly biased estimates, considering the uncertainty of the isochrones and the likely spread of ages. These inaccurate masses serve only for a relative ranking of stars. The mass ratios are

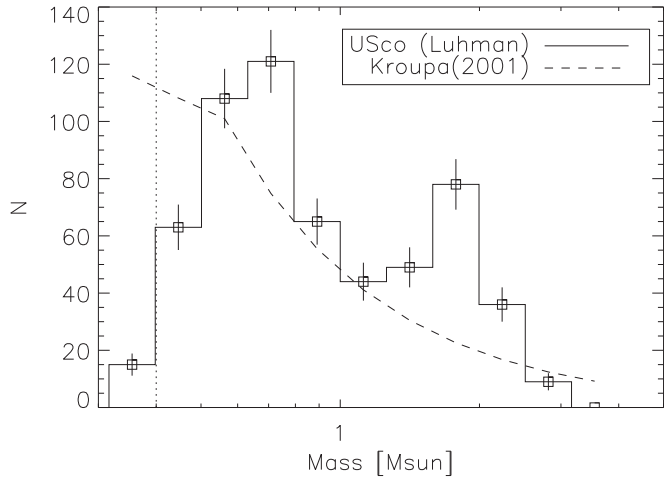

Figure 4. Distribution of estimated masses in our filtered sample. The dashed line is the Kroupa (2001) initial mass function normalized to match the total number of stars. The decline at low mass is a combination of removing faint stars from the filtered sample and its intrinsic incompleteness. The cutoff at 0.4 $\mathcal{M}_\odot$ is shown by the vertical line.

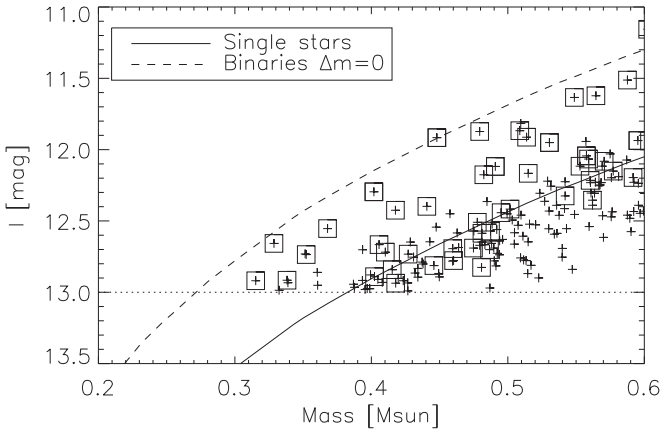

Figure 5. Relation between mass and I magnitude according to the PARSEC 8 Myr isochrone (solid line), assuming a distance of 140 pc. The magnitude cutoff at $I = 13$ mag is shown by the dotted horizontal line, while the dashed line corresponds to the isochrone for binaries with equal components, 0.75 mag brighter compared to single stars. Estimated masses and I magnitudes of the targets are plotted as plus signs, and those of resolved binaries are marked by squares.

estimated from relative photometry using patched isochrones. Here only the local slope of the isochrones matters; hence, the mass ratios are known better than the absolute masses. Masses M_* assigned to unresolved binary stars based on their combined M_V are, on average, slightly larger than the masses of their primary components (see below). In the following, we rank all objects, single and binary alike, using only M_*.

The distribution of points along the main sequence in the CMD in Figure 2 is nonuniform, with less stars around $M_V \sim 6$. The distribution of absolute magnitudes and, correspondingly, masses is nonmonotonic, with a deficit around $\sim$1 $\mathcal{M}_\odot$ (Figure 4). This deficit is also apparent in the distribution of raw magnitudes. K. L. Luhman (2018, private communication) suggested that his sample is incomplete for G-type stars. Indeed, it is difficult to distinguish young G-type stars from the background using the standard criteria of youth, which are more reliable for later spectral types. We noted a similar effect in the RSC18 sample of USco members. However, our control sample of USco members based on the GDR2 has a smooth distribution of both absolute magnitudes and derived masses. The CMDs presented by Damiani et al. (2019) also appear to have a uniformly populated main sequence without gaps. Luhman (2018) discussed an apparent excess of late K-type stars in Taurus relative to the standard initial mass function and concluded that it is not real. Therefore, the relative deficit of solar-mass stars in Luhman's sample of USco members is likely caused by their method of candidate selection. Investigation of this effect is beyond the scope of our work.

The magnitude cutoff $I < 13$ mag in the filtered sample corresponds to a single star of 0.38 $\mathcal{M}_\odot$ at a distance of 140 pc, or $V = 15.9$, $V - I = 2.8$, and $V - K = 5.3$ mag according to the PARSEC isochrone. However, a binary star is brighter than a single star by up to 0.75 mag and may be included in the sample even if its individual components are below the photometric cutoff. This situation, illustrated in Figure 5, creates a bias in favor of low-mass binaries (the Branch bias). Indeed, we note that five stars with $M_* < 0.4$ $\mathcal{M}_\odot$ are resolved binaries; the remaining stars in this region could be tight unresolved pairs, too. However, at a given I magnitude, binaries are redder than single stars, and their masses, estimated from M_V, are below 0.4 $\mathcal{M}_\odot$. By limiting our statistical analysis to stars with $M_* > 0.4$ $\mathcal{M}_\odot$, we avoid the Branch bias caused by the magnitude cutoff imposed on our sample.

3. The SOAR Survey of USco

3.1. Instrument and Data Processing

We used the high-resolution camera (HRCam) on the 4.1 m Southern Astrophysical Research Telescope (SOAR) located at Cerro Pachón in Chile. The instrument, observing procedure, and data reduction are covered in Tokovinin (2018); see the recent results and references in Tokovinin et al. (2018, 2019).

We applied twice for observing time to execute this survey through the NOAO TAC, but the time was not granted. So, we used for this study parts of the engineering nights remaining after completion of the technical work (mostly morning hours) and a fraction of time allocated to other speckle programs remaining as a result of our highly efficient observing procedure. The observations started in 2018 March (these data are partly published in Tokovinin & Briceño 2018) and continued in 2019. Overall, we used about 2 nights of telescope time. Our strategy is to observe all targets, regardless of prior multiplicity surveys.

The survey has been done in the I filter of HRCam (824/170 nm). For each target, two data cubes of 400 frames each were recorded using the 2 × 2 binning (effective pixel scale 31.5 mas) and 200 × 200 binned pixels region of interest (6.″30 on the sky). The exposure time of 25 ms was used for most of the targets; it was increased to 50 ms and even to 100 ms for fainter stars and/or under worse seeing conditions. Some data were also taken without binning in a smaller 3.″15 field.

The data cubes were processed by the SOAR speckle pipeline, jointly with other HRCam data (Tokovinin 2018). Companions are detected by visual inspection of the speckle autocorrelation functions (ACFs) and/or the speckle power spectra, where binary stars are manifested by fringes. Parameters of binary stars (separation ρ, position angle θ, and magnitude difference Δm) and their internal errors are

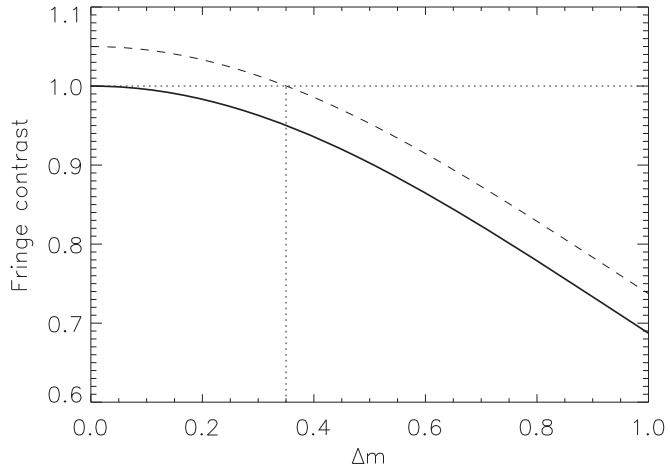

Figure 6. Dependence of the fringe contrast in the speckle power spectrum on the magnitude difference of the binary star Δm. The dashed curve corresponds to a contrast error of +5%.

determined by fitting the power spectra to the binary star model. Two (or more) data cubes of the same target give consistent results in terms of binary star astrometry and relative photometry, while mutual agreement between the cubes provides another estimate of the internal errors. The pixel scale and orientation are calibrated using a set of wide binaries with well-modeled motion, observed in each run together with the main programs.

Small magnitude differences $\Delta m < 0.4$ mag are not measured reliably by speckle interferometry. As shown in Figure 6, in this regime, the contrast of fringes from which Δm is calculated depends on Δm quadratically. An error of the measured contrast by +5%, caused by noise or bias, results in $\Delta m = 0$ assigned to all binaries with $\Delta m < 0.35$ mag. This effect produces an excess of binaries with $\Delta m = 0$ in the SOAR data. Hence, the large mass ratios $q > 0.95$ cannot be reliably determined from the relative speckle photometry. We take this bias into account in our statistical analysis.

Figure 7 illustrates some close binaries in USco discovered at SOAR. Wide companions are better spotted in the ACF, while companions near the diffraction limit are better detected by the elongation of the power spectrum.

Three targets (US0447, US0964, and US1273) are found in nonhierarchical configurations (trapezia) with comparable separations of a few arcseconds between the components (Figure 8). For the first two, images in the full 15.″6 field were taken. The GDR2 astrometry indicates that in all cases, one of the two bright companions is optical and the other is physical; optical companions are marked in Figure 8 by crosses. Two additional faint stars near US0447 are likely optical, too. USco is close to the Galactic equator, where a high density of background stars can produce close asterisms.

3.2. Detection Limits of HRCam

Detection of binary companions in the speckle ACF depends on its fluctuation σ; companions above 5σ are reliably detected, as demonstrated by simulations of artificial companions in Tokovinin et al. (2010). However, the 5σ criterion does not work for very close pairs with separations below ~0.″1, detected as fringes in the power spectrum rather than peaks in the ACF. The resolution is determined by the diffraction limit λ/D (41.5 mas in the I filter), but for faint binaries, it can be

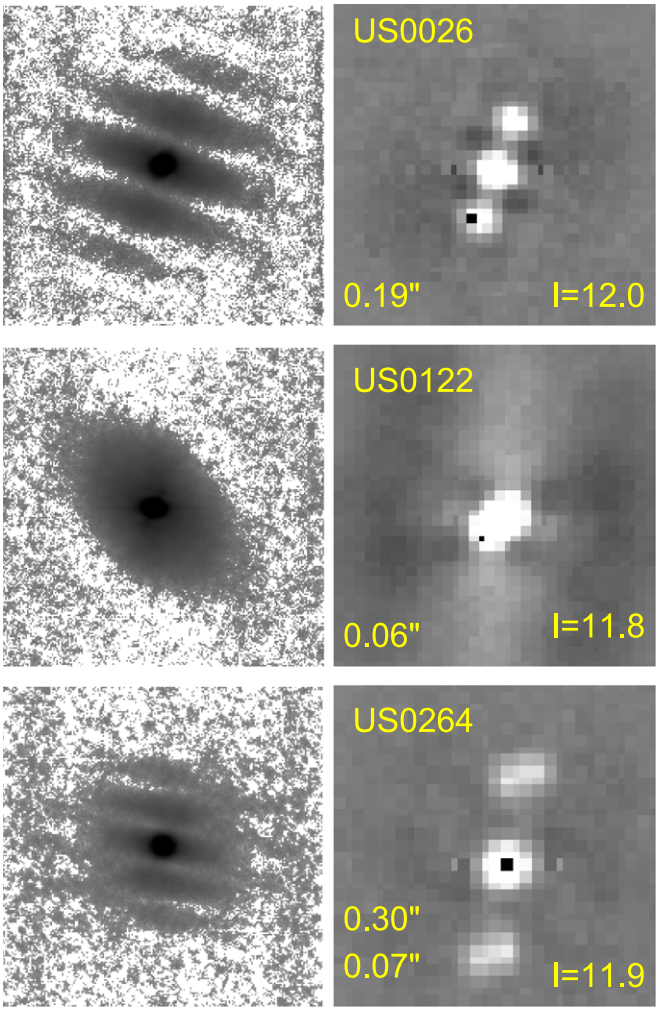

Figure 7. Examples of three new systems discovered in this survey. For each star, identified by its number, the power spectrum is shown on the left (with a negative logarithmic intensity scale) and the ACF on the right in arbitrary scale (companions are marked by black dots). The separations and I-band magnitudes are indicated. The 1.″58 companion to US0122 (KOH 55) is not confirmed by SOAR and *Gaia*. US0264 is a triple system of A, BC and B, C architecture.

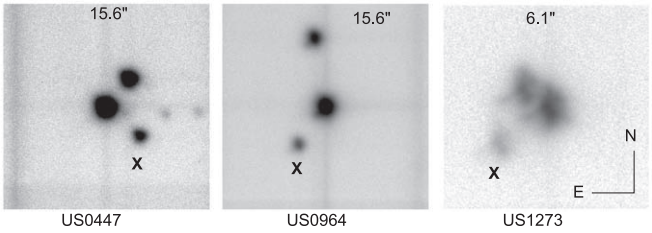

Figure 8. Seeing-limited images of three nonhierarchical asterisms found at SOAR. Crosses mark optical companions with mismatching *Gaia* parallaxes. The angular size of each image is indicated.

worse, depending on the highest spatial frequency where the signal in the power spectrum is above the noise level.

Reliable knowledge of the detection limits is essential for a binary star survey like this one. Therefore, we studied detection of binaries by simulating close companions using the actual power spectra of faint single stars with artificial binary fringes. We found that the effective resolution limit corresponds to $\rho_{\min} = 1/f_{\max}$, where $f_{\max} \leqslant f_c = D/\lambda$ is the maximum spatial frequency containing speckle signal above noise. Simulated

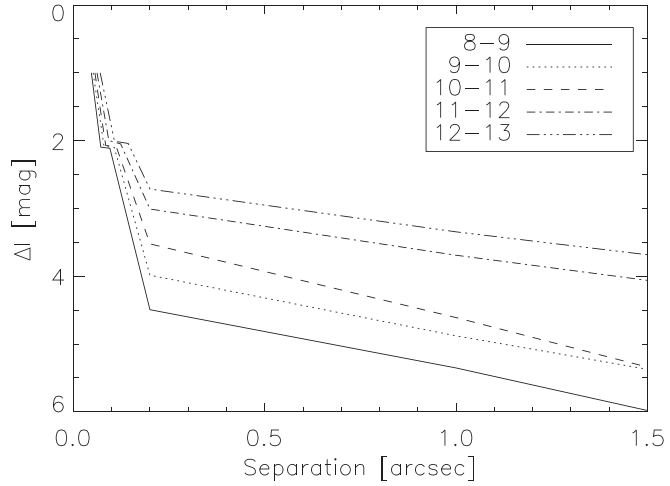

Figure 9. Detection limits for the speckle survey of USco. Median limiting contrast ΔI at six fixed separations for targets grouped by their I magnitude is plotted. Note that the minimum separation also depends on the magnitude. Separations from $0\farcs05$ to $1\farcs5$ project to 7 and 210 au at 140 pc distance.

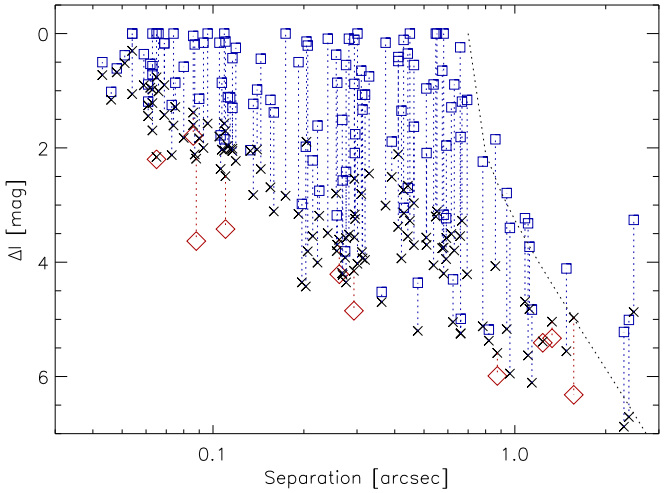

Figure 10. The magnitude difference ΔI of binary companions measured at SOAR is plotted against their separation by blue squares. They are connected by dashed lines to the detection limits for these same stars (black crosses). A few cases where the companions are slightly fainter than the estimated detection limits are highlighted by red diamonds. Companions also measured by *Gaia* are removed from the plot, and the adopted *Gaia* detection limit is shown by the dotted line.

binaries with a separation $\rho_{\rm min}$ and $\Delta m \leqslant 1$ mag are detectable. For wider binaries, the standard 5σ criterion is confirmed.

We modified our speckle pipeline and computed $\rho_{\rm min}$ for all data cubes. The maximum detectable magnitude difference depends on the binary separation, star brightness, and, of course, the seeing that influences the strength of the speckle signal. Figure 9 shows the median detection limits at six fixed separations, grouped by the I magnitude of the targets. Note that the minimum separation (the first point) also depends on the target magnitude. Under typical conditions, the resolution is noticeably lost at $I > 12.5$ mag, setting the limit of our survey.

The statistical analysis below uses the individual detection limits for each target. They are selected as the best limits among available data cubes. We checked that the detected binary companions are actually above the limits (Figure 10). There are a few exceptions where the companions are fainter than the estimated limit. However, we should bear in mind that the probability of companion detection is a smooth function of Δm and ρ, not a step function. The dotted line marks the *Gaia* detection limit. Three companions located in this area are not found in GDR2 but recovered at SOAR.

3.3. Table of SOAR Results

The results of the observations with HRCam at SOAR are presented in the electronic Table 2. Its columns contain: (1) the Washington Double Star Catalog (WDS) code based on J2000 coordinates (for objects that are not present in the WDS, these codes were created); (2) the source number USn from E18, same as in Table 1; (3) the discoverer name and, if necessary, component designation, taken from the WDS for resolved known pairs or derived from the USn numbers otherwise. The following columns give (4) Julian year of observation, (5) filter, (6) position angle, (7) separation, (8) error of separation, and (9) magnitude difference. For unresolved sources, all parameters are zero. The relative photometry and astrometry of resolved triples refers to pairings between individual components as indicated (e.g., A,B and B,C, but not A,BC). The last three columns give (10) the minimum detectable separation $\rho_{\rm min}$, (11) the maximum detectable magnitude difference at $0\farcs15$, and (12) the same at $1''$. More detailed information is presented in the merged table of detection limits described below.

Table 2
Results of SOAR Observations

Col.	Label	Format	Description, Units
1	WDS	A10	WDS code (J2000)
2	USn	I4	Number in E18
3	Name	A16	Discoverer code or name
4	Date	F8.3	Date of observation, JY
5	Filt.	A2	Filter
6	θ	F6.1	Position angle, deg
7	ρ	F8.3	Separation, arcsec
8	σ_ρ	F7.1	Error on ρ, mas
9	Δm	F6.2	Magnitude difference, mag
10	$\rho_{\rm min}$	F7.3	Min. separation, arcsec
11	$\Delta m_{0.15}$	F7.2	Max. Δm at $0\farcs15$, mag
12	Δm_1	F7.2	Max. Δm at $1''$, mag

(This table is available in its entirety in machine-readable form.)

The data assembled in Table 2 come from a variety of observing programs executed with HRCam. They include observations of multiperiodic stars published by Tokovinin & Briceño (2018), observations of binaries with orbital motion, etc. We omitted several redundant observations taken before 2016. Some stars were visited more than once, because they either belonged to different programs or were followed to confirm the discovery or detect the orbital motion. Overall, Table 2 contains 706 rows with 187 resolved pairs or subsystems; 89 resolutions are new (34 of those are also found in GDR2), and another 29 are published by Tokovinin & Briceño (2018). Almost half of the USco binaries known today (118 out of 250) were discovered at SOAR. The total number of processed data cubes is 1536. All 614 targets have been observed at least once.

Many close pairs in USco discovered here have short estimated periods. Their orbits can be determined within a few years, yielding masses for testing the evolutionary tracks of

Table 3
Detection Limits

Col.	Label	Format	Description, Units
1	USn	I4	Number in E18
2	Ref.	A8	Reference[a]
3	Meth.	A3	Method[b]
4	λ	F6.2	Imaging wavelength, μm
5–10	ρ_i	F6.3	Separations, arcsec
11–16	Δm_i	F6.2	Maximum Δm, mag

Notes.
[a] See Table 4.
[b] Methods: AO—adaptive optics; SI—speckle interferometry; q—mass ratios are given instead of Δm.

(This table is available in its entirety in machine-readable form.)

young stars. The fast orbital motion of some pairs is evidenced by repeated measurements at SOAR taken within a year.

4. Binary Stars in USco

In this section, we combine the results of our SOAR survey with the previously available data and information from GDR2 to produce a catalog of 250 physical binary stars in USco for subsequent statistical analysis.

4.1. Previous Surveys

The statistical analysis presented below does not rely entirely on the SOAR data and includes the results of previous multiplicity surveys in USco. The binaries detected in these surveys or known from the era of visual observers are included in the general list. We also take into account the number of targets and the detection limits of each survey. The detection limits are defined here as the maximum detectable Δm_i at six separations ρ_i. The first separation corresponds to the angular resolution $\rho_{\min}$ and the last to the maximum surveyed separation (usually half of the imaging field size). The detection limits are linearly interpolated between ρ_i and, knowing the imaging wavelength, can be converted into the minimum detectable mass ratios $q_{\min}(\rho)$ for each of our targets using the isochrones. All detection limits are assembled in Table 3.

Figure 11 illustrates the combined detection limits for one of our targets, US0197 ($M_* = 0.56\,\mathcal{M}_\odot$, $I = 12.6$ mag). It has been observed at high angular resolution by Koehler et al. (2000) and at SOAR; the latter detected a companion at $\rho = 0\farcs43$ with $\Delta I = 3.05$ mag, which, in principle, could also be found by Koehler et al. At separations beyond $1''$, *Gaia* has a deeper detection limit compared to speckle imaging.

Table 4 summarizes in compact form relevant imaging surveys of USco in chronological order. It gives the number of targets N belonging to our sample, the imaging wavelength λ in microns, and the angular resolution $\rho_{\min}$ in arcseconds. For each publication, the corresponding electronic table was retrieved, read by a specially written IDL program, cross-matched with the sample by coordinates, and exported in the standard format (ρ_i and Δm_i) into a text file. When the number of detection limits given in the paper is less than six, the last limits are duplicated. When the number is larger than six, we use the first five closest separations and the last widest separation. Short comments on each survey are provided in the rest of this section. The present sample exceeds previous samples by an order of magnitude.

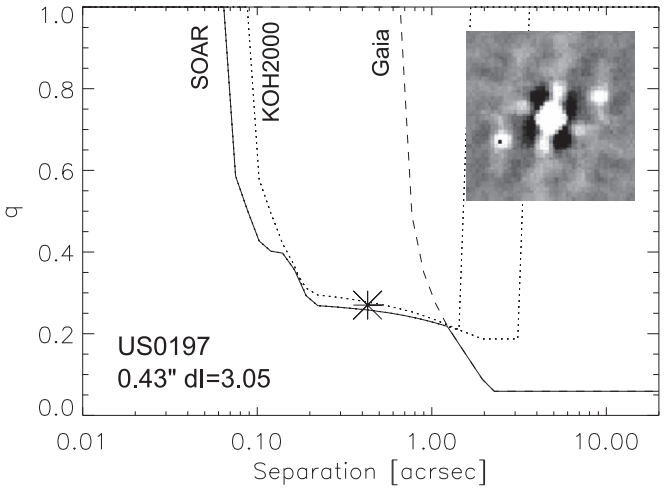

Figure 11. Limits of companion detection around US0197. The faint companion at $0\farcs43$ with $q = 0.27$ is marked by a large asterisk; the corresponding ACF is shown in the insert, where the black dot marks the companion. Secondary spikes in the ACF are artifacts.

Koehler et al. (2000) performed the pioneering survey of USco and other young associations using speckle interferometry in the K band at the ESO 3.5 m New Technology Telescope. For all of their targets, we adopt the fixed detection limits from Figure 3 of their paper: $\rho_i = [0.06, 0.1, 0.13, 0.6, 1.0, 6.0]$ arcsec, $\Delta m_i = [0.0, 2.5, 3.0, 4, 4.5, 5.0]$ mag.

Kouwenhoven et al. (2005) surveyed relatively bright stars of spectral types B, A, and F with adaptive optics (AO). They used the ADONIS AO system on the 3.6 m ESO telescope at La Silla. All targets were observed in the K band, and some were also observed in the J and H bands. Here we use only the K-band data (they are deeper in mass ratio but lower in resolution). Their paper does not provide the individual detection limits, only the summary plot in their Figure 3 with an empirical limiting line. We reproduced a similar plot from their data on resolved companions and adopted the upper envelope as the relevant detection limit: $\rho_i = [0.2, 0.5, 1, 2, 5, 10]$ arcsec and $\Delta m = [0.5, 2.7, 5, 7, 8, 8]$ mag. The detection depth at large separations does not matter because we confirm wide companions using *Gaia*.

Metchev & Hillenbrand (2009) observed young stars, including several USco members, in the K band using AO at the Palomar and Keck telescopes. We adopt fixed detection limits: $\rho_i = [0.09, 1.0, 2.0, 5.0, 5.0, 5.0]$ arcsec and $\Delta m_i = [0.0, 17.2, 19.4, 20.3, 20.3, 20.3]$ mag.

Kraus & Hillenbrand (2012) published a compilation of multiplicity surveys in USco done both with AO and at the seeing-limited resolution. Individual detection limits are retrieved from their Table 7 that lists minimum mass ratios versus projected separations in au for each star individually. The data are ingested as published, with separations converted back to angular units. We assume that earlier works by this group are included in this compilation and do not consult their earlier papers.

Lafrenière et al. (2014) observed 91 stars in USco with the AO instrument at the Gemini North telescope. Their input sample was based on the same list of bright USco members used by prior surveys; hence, there is a large number of targets in common with prior work. We use the data from their Tables 1 and 2 that provide individual limits for each target. Lafrenière et al. noted that the multiplicity fraction does not

Table 4
Multiplicity Surveys of USco

Label	Reference	N	λ (μm)	$\rho_{\min}$ (arcsec)	Method[a]
KOH2000	Koehler et al. (2000)	41	2.2	0.06	SI
KOU05	Kouwenhoven et al. (2005)	50	2.2	0.2	AO
MH09	Metchev & Hillenbrand (2009)	16	2.2	0.1	AO
KRS12	Kraus & Hillenbrand (2012)	44	2.2	Var.	AO, seeing
LAF14	Lafrenière et al. (2014)	73	2.2	0.10	AO
SOAR	This work	614	0.8	0.05	SI

Note.
[a] Methods: SI—speckle interferometry; AO—adaptive optics; seeing—seeing-limited.

decline with mass (unlike stars in the field) and that binaries with comparable masses and large separations are rare. Below, we confirm both of their conclusions for our much larger sample.

Several publications are not considered in the table of detection limits; they are commented on briefly.

Shatsky & Tokovinin (2002) observed 115 stars of spectral types O and B in the Sco OB2 association, including USco. However, none belong to our sample.

Bouy et al. (2006) observed low-mass members of USco and resolved some multiple systems. Unfortunately, their paper does not contain the list of all observed targets and the detection limits. None of these binaries are present in our list of resolved pairs.

Janson et al. (2013) observed 138 bright stars in the Sco–Cen region, not covered by prior work, using the NICI AO instrument at Gemini South. Examination of their Table 1 reveals no matches with our sample. Interestingly, they found a total absence of relatively wide pairs with small Δm, an effect likely caused by the construction of their sample that avoided known binaries from the outset.

Hinkley et al. (2015) used high-contrast imaging and detected faint companions to three stars in USco, two of which, HIP 78196 (US0193) and HIP 79124 (US0708), belong to our sample. They do not provide a list of all observed targets.

Our sample contains 126 targets with *Hipparcos* numbers. The limits of companion detection by *Hipparcos* are adopted in the same way as for the 67 pc sample of solar-type stars (Tokovinin 2014): ρ_i = [0.09, 0.14, 0.4, 1, 5, 10] arcseconds, Δm_i = [0, 2.2, 4.0, 4.1, 4.2, 4.3] mag, wavelength 0.5 μm.

4.2. *Binaries in the* Gaia *DR2*

As mentioned above, all sources within 20″ from our targets were retrieved from the GDR2 catalog (Gaia Collaboration et al. 2018). Figure 12 shows the magnitude difference versus separation for all *Gaia* pairs. The lower envelope is approximated by the formula

$$\Delta G(\rho) = 5.5(\rho - 0.7)^{0.4}, \quad \rho > 0\farcs7, \tag{3}$$

which describes the *Gaia* detection limit. Similar limits for companion detection in *Gaia* were derived by Brandeker & Cataldi (2019). By companions, we mean here both the real (physical) binaries and the random optical pairs, according to the established double star terminology. In addition to the contrast limit, stars fainter than $G = 20.5$ mag are not present in GDR2, reducing the number of pairs with large ΔG. The GDR2 magnitude limit, relevant for faint targets, is accounted for by our model of *Gaia* companion detection.

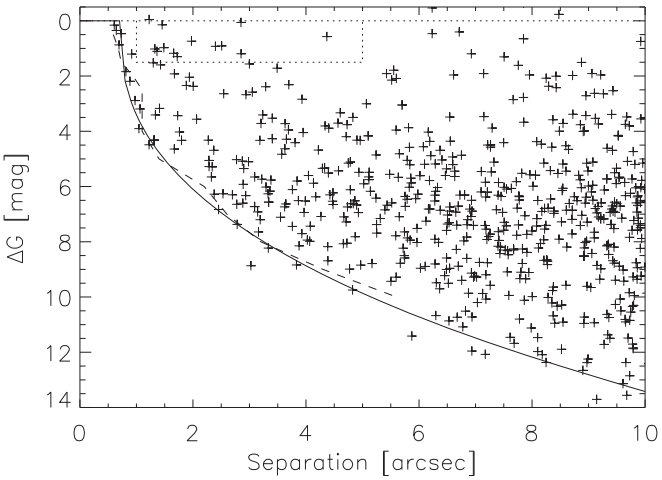

Figure 12. Magnitude difference ΔG vs. separation for all companions in *Gaia* DR2 found near our targets. The solid line is the adopted detection limit according to Equation (3), and the dashed line is the 50% detection limit from Brandeker & Cataldi (2019). The dotted rectangle indicates the zone of blended targets.

Naturally, the majority of companions in Figure 12 are unrelated (optical) stars. The average number of companions per target with $\Delta G < 5$ mag and separation less that ρ grows quadratically as $N_{\Delta G<5}(\rho) \approx 0.81(\rho/20'')^2$. According to this formula, we expect to find five optical companions with $\Delta G < 5$ mag and $\rho < 2''$ in the whole sample; the actual number of such *Gaia* pairs is 40.

We consider all *Gaia* pairs with $\rho < 2''$ as potentially physical. Some (but not all) of these close pairs are classified as physical or optical because parallaxes of the companions are present in GDR2. Most close *Gaia* companions are also detected at SOAR and confirmed as physical (comoving), with a few exceptions, like US1353. The wider *Gaia* companions with $\rho > 2''$ are accepted as physical only if they have astrometric data in GDR2 that confirm their membership in USco. Wide companions that are themselves close pairs and hence lack *Gaia* astrometry are excluded from our survey.

There are 40 pairs wider than 0.″6 detected by both *Gaia* and SOAR. Their angular separations match very well. The median offset $\rho_{\rm SOAR} - \rho_{Gaia}$ is 9 mas, and its rms scatter is 10 mas after removing the optical pair US1353 (its companion has moved by 63 mas between 2015.5 and 2019.2). The magnitude differences are also in good agreement, with $\Delta I \approx 0.96\Delta G$ (line in Figure 13). However, two pairs (US0820 and US1081)

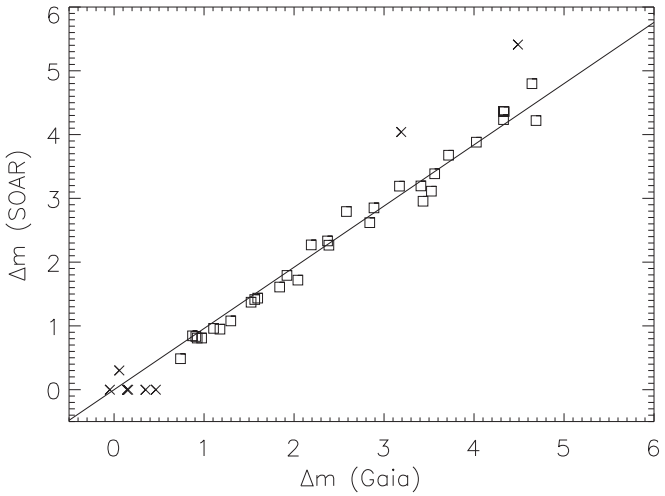

Figure 13. Comparison between the relative photometry of pairs measured by *Gaia* and at SOAR. The outliers are marked by crosses, and the line is $\Delta I = 0.96\Delta G$.

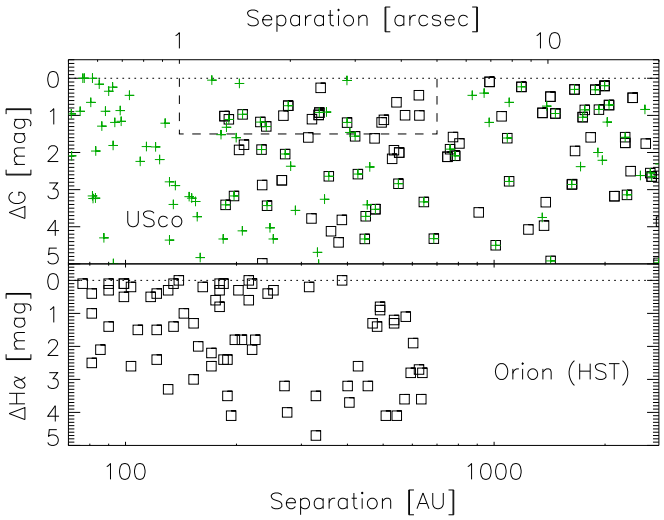

Figure 14. Magnitude difference vs. separation. The upper plot shows pairs of USco members in the control GDR2 sample (squares). For comparison, pairs in our binary catalog are plotted by green plus signs. The regime of blended targets is outlined by the dashed rectangle. The lower plot refers to binaries in Orion from Table 1 of Reipurth et al. (2007) discovered with the *Hubble Space Telescope*.

plotted by crosses have a substantially larger ΔI measured at SOAR; their separations are around 1″. The latter was observed in a small 3.″15 field where the relative photometry could be biased by vignetting. Photometric variability of some companions (flares or dimmings) cannot be ruled out because these stars are young. We note that speckle photometry has a tendency to underestimate small $\Delta I < 0.5$ mag by assigning $\Delta I = 0$, as noted above (see Figure 6). We use the *Gaia* photometry when it is available.

Some wide *Gaia* pairs consist of two members of our sample. In this case, the secondary components are marked in Table 1 and not counted as separate targets, with a few exceptions, like trapezia, discussed below. Targets US0432 and US0613 are paired to USco members that are not present in Luhman's sample at separations 16.″2 and 19.″0 and brighter by 1.7 and 0.5 mag, respectively. These pairs are not included in our binary catalog. However, the companion to US1248 at 8.″5, 0.23 mag brighter, is included with $\Delta G = 0.23$ mag.

4.3. Binaries in the WDS

We retrieved all known pairs in our sample from the WDS (Mason et al. 2001). Only pairs with $\rho < 20''$ and $\Delta m < 6$ mag are considered to avoid numerous optical pairs. High-contrast imaging revealed many faint companions around some USco stars, all faithfully recorded in the WDS and most of them optical. We keep only the binaries proven to be physical by *Gaia* and ignore the rest. Pre-*Gaia* multiplicity surveys might have included some optical pairs and hence overestimated the multiplicity. The majority of WDS binaries are also detected at SOAR and/or by *Gaia*, and we use the literature data for only 16 systems. Most of those are close pairs with a large contrast discovered by aperture masking and undetectable at SOAR. Their parameters are outside the range of separations and mass ratios studied here, but we keep these pairs for completeness. A few unconfirmed WDS binaries (e.g., those discovered by lunar occultations) are omitted.

4.4. Blended Targets

In the following, we note the paucity of USco binaries with separations of a few arcseconds and nearly equal components. When we first saw this effect in the sample of RSC18, there was a suspicion that such stars were removed from the *Kepler K2* campaign as unsuitable for precise photometry. Luhman's sample, being independent of *Kepler*, still uses photometry and astrometry that could be affected by the resolved nature of some stars, leading to the rejection of blended targets. For example, semi-resolved stars are missing from the 2MASS point-source catalog. These stars are not suitable as references for AO systems and could be removed from AO-based multiplicity surveys. For brevity, we call binaries with $1'' < \rho < 5''$ and $\Delta m < 1.5$ mag (this corresponds roughly to $q > 0.7$) *blended targets*. To prove the reality of the deficit of wide binaries with similar components in USco, we must verify that the input sample is not biased against blended targets.

To address this concern, we selected from the WDS all pairs in the area covered by Luhman's sample, with PMs within ±10 mas yr^{-1} from the mean PM of USco and separations $\rho < 20''$. The resulting list was cross-matched with GDR2. The subset of WDS pairs in the blending regime was examined manually to reject nonmembers of USco (based on parallax) and optical pairs, leaving only six physical pairs. Three of those are present in our binary catalog, one is too faint, and two could indeed be the missed blended targets. Their WDS codes are 16116−1839 and 16256−2327, primary G magnitudes 12.37 and 5.54 mag, separations 1.″3 and 3.″0, $\Delta m = 0.50$ and 0.67 mag. For consistency, we do not add those targets to Luhman's sample.

The *Gaia* census of stars offers an independent check of potential bias against blended targets. All such pairs are easily detectable by *Gaia* (see the dotted rectangle in Figure 12). Using our control sample of 664 USco members based exclusively on GDR2, we found 18 pairs in the blending regime. They are plotted in Figure 14; 16 of them are confirmed as physical by *Gaia* astrometry of the companions, and two have unknown status. For comparison, our binary catalog based on Luhman's sample contains 13 blended targets among 604 systems (one optical pair is removed from the catalog). The numbers and relative frequencies of the blended targets in both samples are consistent within the statistical errors. We also used the sample of USco members derived from the lists of

Table 5
List of Binaries in USco

Col.	Label	Format	Description, Units
1	WDS	A10	WDS code (J2000)
2	USn	I4	Number in E18
3	Name	A16	Discoverer code or name
4	Date	F8.2	Date of observation, yr
5	θ	F6.1	Position angle, deg
6	ρ	F8.3	Separation, arcsec
7	Δm	F6.2	Magnitude difference, mag
8	λ	F6.2	Wavelength, μm
9	m_1	F6.2	Primary mass, $\mathcal{M}_\odot$
10	q	F6.3	Mass ratio
11	L	I2	Hierarchical level

(This table is available in its entirety in machine-readable form.)

Damiani et al. (2019) and reached the same conclusion. Luhman's sample cannot miss more than a few blended targets, if any. We infer that its bias against blended targets is insignificant, and the paucity of such binaries is real.

The paucity of near-equal binaries with separations of a few hundred au, compared to smaller and larger separations, may exist in other star-forming regions, for example, the Orion Nebular Cluster (ONC) studied by Reipurth et al. (2007). These authors noted a sharp decline in the binary frequency at separations >225 au and related it to the dynamical disruption of wide binaries in the dense cluster. However, 10 pairs out of 78 in their Table 1 have $\Delta m < 2$ mag and projected separations $s > 500$ au (see the lower panel of Figure 14). These binaries are likely physical (wide optical pairs tend to have large Δm). Therefore, relatively wide binaries with comparable components exist in the ONC, as well as in USco. However, in both regions, such pairs are rare at intermediate separations from 200 to 500 au.

4.5. Combined List of Binary Stars

The lists of companions from three sources, *Gaia*, SOAR, and WDS, were merged and examined to produce the final list of binaries in Table 5, selecting from multiple sources in this order of preference. The first three columns are similar to those of Table 2. Then follow the date, position angle θ, separation ρ, magnitude difference Δm, and wavelength λ to which it refers (0.6 μm for *Gaia*, 0.8 μm for SOAR in the *I* filter). Columns (9) and (10) contain the estimated mass of the primary component (the contribution of the secondary to the combined light of close pairs is accounted for) and the mass ratio. Column (11) codes the hierarchy (level 1 for outer systems, level 11 for inner subsystems around primary, level 12 for secondary subsystems). We estimated mass ratios from the patched PARSEC 8 Myr isochrones as follows. The isochrone in the photometric band closest to the imaging λ is selected. The absolute magnitude in this band is computed from the crude mass M_* estimated for this target in the main sample. The absolute magnitudes of both components are computed from the measured Δm, accounting for the contribution of the secondary component to the combined light for close pairs unresolved by *Gaia* (remember that the *V* magnitudes are derived from the *Gaia* photometry). The masses of both components are interpolated back from the same isochrone. As expected, for some close pairs, the primary mass m_1 is less than M_*, but the difference is typically small. The median ratio m_1/M_* is 0.99, and the minimum ratio is 0.7. We consistently use M_* for ranking all stars in mass.

Seven subsystems belonging to the secondary components of wider pairs (level 12) are included in our analysis. However, their mass M_* is set to the secondary mass m_2 of the outer pair. Three of those subsystems fall below our cutoff at 0.4 $\mathcal{M}_\odot$, and the remaining four contribute to the statistics at their masses, not at the masses of the wide primary components. There are also 11 subsystems of level 11 belonging to the primary components of wider pairs.

The list contains 250 pairs, counting all subsystems separately. A large number of physical pairs, 70, were found in *Gaia* (discovery code GAnnnn, where nnnn is the number in E18); 34 of those are independently confirmed at SOAR. We also used *Gaia* to discard some optical companions listed in the WDS. When the WDS and SOAR pairs were also measured by *Gaia*, the latter data are preferred; they are distinguished by the date of 2015.5 and $\lambda = 0.6$ μm. Overall, 102 pairs have *Gaia* relative astrometry and photometry. We provide additional comments on some binaries in the Appendix.

The catalog includes 28 binaries from Tokovinin & Briceño (2018) with discoverer codes TOK* assigned to them by the WDS, as well as another 55 pairs resolved at SOAR later (names starting with US). All measurements of SOAR pairs are listed in Table 2. The remaining 97 pairs with various discoverer codes were known from previous work. Most of them are confirmed by *Gaia* and/or SOAR. We prefer the SOAR measurements over those given in the WDS and give them for 132 close pairs unresolved by *Gaia*. Only 16 pairs in Table 5, unresolved by both *Gaia* and SOAR, have relative astrometry and photometry retrieved from the literature.

5. Binary Statistics

In this section, we study the joint distribution of binary separations and mass ratios in USco, taking into account the detection limits. The mass ratios are estimated from the magnitude differences using the isochrones, as explained above, while the angular separations are translated into linear projected separations $s = \rho d$, assuming the common distance $d = 140$ pc. We consider all binaries regardless of their hierarchy, i.e., include subsystems of levels 11 and 12. The binaries are grouped according to their masses M_* and separations ρ. The companion star fraction (CSF) is the binary fraction in the corresponding group after accounting for the incompleteness.

Figure 15 plots the separations and mass ratios overlaid on the detection probability for the full sample. The detection power is sufficient to study binaries with $q > 0.3$ at projected separations s from ~10 to 2800 au. Figure 15 clearly shows that the distribution of the mass ratio depends on separation. Binaries with $q > 0.7$ are rare at separations from 1″ to 5″ but present at smaller and larger separations. This effect is quantified in the following subsections.

5.1. Distribution of the Mass Ratio

Following Moe & Di Stefano (2017), we model the mass ratio distribution by the truncated power law $f(q) \propto q^{\gamma_{0.3}}$ in the range $[q_{\min}, q_{\max}]$. Looking at Figure 15, we note little detection power for close pairs with $q < 0.3$ and adopt the modeled range of [0.3, 1], as in the above paper. Note that the q range is, implicitly, also a model parameter, and $\gamma_{0.3}$ depends

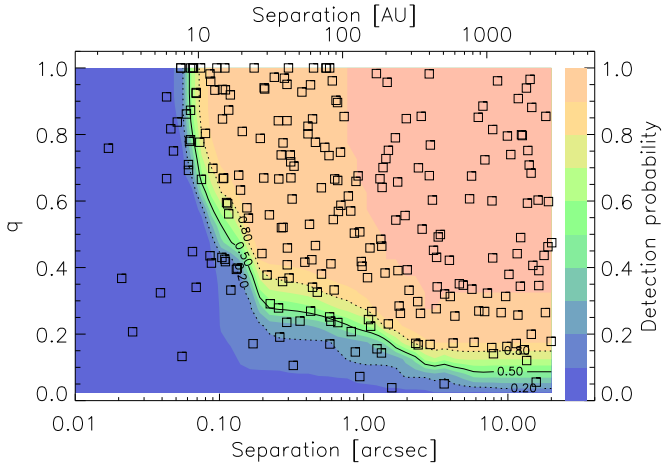

Figure 15. Mass ratio vs. separation for all binaries in our sample. The colors represent the average detection probability from zero to 1 (color bar and scale on the right); its contours at the 0.2, 0.5, and 0.8 levels are overplotted.

on it. The model is the truncated power law, not the general power law. We also model the separate population of twin binaries with the mass ratios uniformly distributed between 0.95 and 1. It is characterized by the twin fraction $f_{\rm twin}$, i.e., the excess of twins with respect to the power law, relative to all binaries with $q > 0.3$, in conformity with the definition used by Moe & Di Stefano (2017). The analytic model also includes the binary fraction ϵ to correctly account for undetected companions.

The parameters of the $f(q)$ model (ϵ, $\gamma_{0.3}$, $f_{\rm twin}$) and their confidence limits are determined by the maximum likelihood (ML) method, as in Tokovinin (2014). The likelihood function $\mathcal{L}$ is

$$\mathcal{L} = 2Nf_0 - 2\sum_{i=1}^{K} \ln(f(q_i)d_i), \quad (4)$$

where N is the sample size, q_i are the mass ratios of K binaries, and d_i are the detection probabilities for these pairs. The probability of companion detection for the complete sample is

$$f_0 = \int_{q_{\rm min}}^{q_{\rm max}} f(q)d(q)dq. \quad (5)$$

It is important to realize that the calculation of f_0 uses all stars in the chosen subsample, not only binaries, to statistically account for undetected companions. The integral in Equation (5) is evaluated numerically on a discrete q grid. The confidence limits of 68% (1σ) and 90% correspond to the hypersurface of $\mathcal{L}$ defined by the increments of 1.0 and 2.17 above its minimum (Press et al. 1986). The ML code was tested using simulated binary samples filtered by simulated incomplete detection to verify that it recovers known parameters of $f(q)$. The excessive number of binaries with $q = 1$ resulting from the speckle photometry bias (excess of $\Delta m = 0$) is dealt with by distributing these mass ratios uniformly in the interval [0.95, 1.0]. We cannot measure these mass ratios accurately, but we know that they are close to 1.

We fit the mass ratio distribution for binaries in the selected ranges of separation and primary mass. The detection limits, computed initially for the complete sample, are filtered accordingly to match only the chosen subsample.

Table 6
Parameters of the Mass Ratio Distribution

Mass Range ($\mathcal{M}_\odot$)	Sep. Range (arcsec)	N_b	$\gamma_{0.3}$	$f_{\rm twin}$
0.4–1.5	0.05–0.25	40	1.50 ± 0.62	0.15 ± 0.08
0.4–1.5	0.25–1.25	47	0.43 ± 0.49	0.13 ± 0.07
0.4–1.5	1.25–20	50	−0.18 ± 0.37	−0.04 ± 0.03
0.4–1.5	0.1–1.0	65	0.60 ± 0.42	0.09 ± 0.05
0.4–1.5	1.0–10	37	−0.72 ± 0.46	0.00 ± 0.04
0.4–0.7	0.05–1.25	44	0.20 ± 0.54	0.23 ± 0.07
0.7–1.5	0.05–1.25	43	1.50 ± 0.55	0.05 ± 0.07
1.5–10	0.05–1.25	23	−1.27 ± 0.59	0.00 ± 0.04
0.4–1.5	0.1–20	137	0.41 ± 0.28	0.08 ± 0.04

The fitted parameters of $f(q)$ are given in Table 6 for stars in several ranges of separations and masses. The third column gives the number of pairs N_b in the chosen intervals. The cumulative plots in Figure 16 demonstrate that the analytical models adequately describe the data. We note that at large separation the fraction of twins decreases and low-mass companions become more frequent, $\gamma_{0.3}$ decreases. We experimented by selecting different ranges of separation and mass and found this trend to be very robust. We also see how $f(q)$ in the fixed separation range evolves with mass: $f_{\rm twins}$ decreases with mass, while $\gamma_{0.3}$ increases and decreases. When a wide range of separations and masses is selected, $f(q)$ becomes almost uniform (see the last line in Table 6).

5.2. Separation Distribution and Companion Frequency

We computed the frequency of binary companions with $q > 0.3$ per decade of separation, f_i, in five logarithmic separation bins of 0.5 dex width between $0\farcs063$ and $20''$ (9–2800 au) by counting the number of companions n_i and dividing it by the product of sample size N, average detection probability d_i, and bin width: $f_i = n_i/(0.5Nd_i)$. These numbers are reported in Table 7. The detection probability is ∼0.7 only in the first bin; at wider separations, the detection of binaries with $q > 0.3$ is nearly complete (see Figure 15). The fraction of companions per decade of separation is plotted in Figure 17 for three intervals of mass. The plots are computed with a sliding bin of 0.5 dex width; hence, the adjacent points are not statistically independent. Typical errors are shown for three bins. The last two lines of Table 7 give the frequency of companions with $q > 0.3$ in the first 1 dex bin in the full separation range of 2.5 dex.

For comparison, we use the lognormal separation distribution of field solar-type binaries within 25 pc from Raghavan et al. (2010; median $\log_{10}(P/1d) = 5.0$, $\sigma_{\log P} = 2.3$ dex, companion fraction CSF = 0.60 ± 0.04) converted into the distribution of semimajor axis for a system mass of 1.5 $\mathcal{M}_\odot$. The mass ratio distribution of solar-type binaries is almost uniform for $0.05 < q < 1$, independent of the period (Tokovinin 2014). Therefore, the fraction of companions with $q > q_{\rm lim}$ is $\mathrm{CSF}_{\rm qlim} = \mathrm{CSF} \times (1 - q_{\rm lim})/0.95$, or 0.44 for $q > 0.3$. M. Moe (2019, private communication) confirmed that CSF = 0.44 is adequate for solar-type binaries with $q > 0.3$. The binary fraction of M-type dwarfs in the field is taken from the work of Winters et al. (2019). We adopt a CSF of 0.35 ± 0.02 to account for the larger binary fraction in the early M stars, guided by Figure 19 of their paper. The lognormal separation distribution peaking at 20 au with a width of 1.16 dex is used. Considering that M-type binaries prefer large q, we do not

Table 7
Fraction of Companions with $q > 0.3$ per Decade of Separation

Separation		0.4–0.7 $\mathcal{M}_\odot$ ($N = 210$)				0.7–1.5 $\mathcal{M}_\odot$ ($N = 209$)				1.5–10 $\mathcal{M}_\odot$ ($N = 153$)		
(arcsec)	(au)	n_i	d_i	f_i	$f_{\rm field}$	n_i	d_i	f_i	$f_{\rm field}$	n_i	d_i	f_i
0.06–0.20	16	17	0.67	0.23 ± 0.06	0.118	11	0.66	0.16 ± 0.05	0.106	11	0.58	0.25 ± 0.07
0.20–0.63	50	18	0.97	0.17 ± 0.04	0.112	22	0.97	0.22 ± 0.05	0.114	8	0.91	0.12 ± 0.04
0.63–2.0	160	14	0.99	0.13 ± 0.03	0.088	9	1.00	0.09 ± 0.03	0.111	7	0.98	0.09 ± 0.03
2.0–6.3	500	4	1.00	0.04 ± 0.02	0.058	11	1.00	0.11 ± 0.03	0.096	6	1.00	0.08 ± 0.03
6.3–20	1600	10	1.00	0.09 ± 0.03	0.032	14	1.00	0.13 ± 0.04	0.076	6	1.00	0.08 ± 0.03
0.06–0.63	28	35	…	0.20 ± 0.04	0.115	33	…	0.19 ± 0.03	0.110	19	…	0.18 ± 0.04
0.06–20	…	63	…	0.33 ± 0.04	0.204	67	…	0.35 ± 0.04	0.252	38	…	0.31 ± 0.05

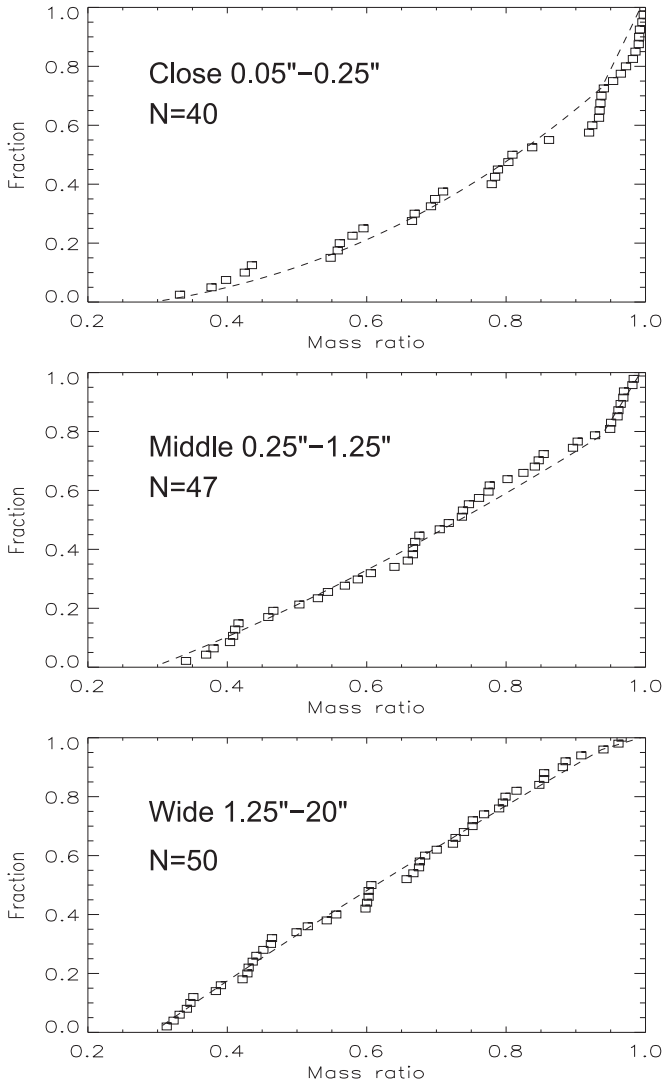

Figure 16. Cumulative distributions of the mass ratio (squares) at $q > 0.3$ and their analytical models (dashed lines) in three ranges of separations for stars with $0.4\ M_\odot < M_* < 1.5\ \mathcal{M}_\odot$.

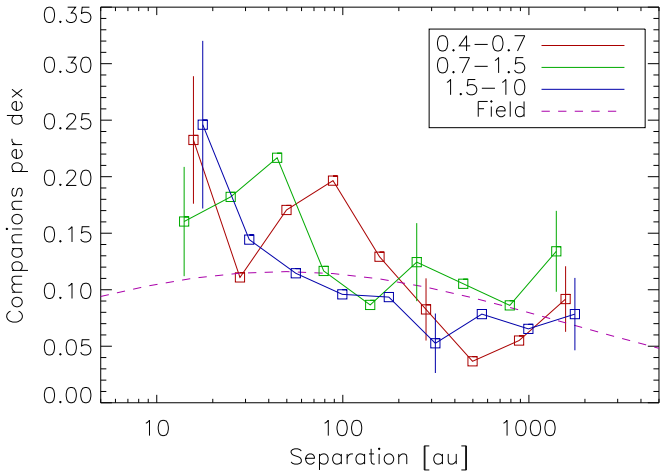

Figure 17. Distribution of separations for binaries with $q > 0.3$ in three mass intervals: 0.4–0.7, 0.7–1.5, and 1.5–10 $\mathcal{M}_\odot$ (see the legend box). Each point corresponds to the 0.5 dex wide separation bin. The bin limits are chosen with a step of 0.25 dex; hence, the adjacent points are not independent. The dashed curve corresponds to the field solar-type binaries. Representative error bars are shown for three bins.

apply any correction while comparing to M-type binaries with $q > 0.3$ in USco. The companion frequency for early M- and solar-type field stars from the cited publications is reported in Table 7.

Strictly speaking, the incompleteness correction depends on $f(q)$, and our formula is valid only for a uniform $f(q)$; for a rising $f(q)$, we overcorrect. When we adopt $f(q)$ with $\gamma_{0.3} = 1$ and $f_{\rm twin} = 0.15$ at separations below $1''$ for the first two mass bins and repeat the calculation, the companion frequency in the first line of Table 7 decreases by ∼0.02, from 0.23 to 0.21 and from 0.16 to 0.14. The overall companion frequency in the full studied separation range also drops by 0.02. There is no effect at wider separations, where the detection probability is high. We report the results without correcting for $f(q)$, i.e., assume a flat $f(q)$.

The projected separation s equals the semimajor axis a statistically, and the scatter of $\log_{10}(s/a)$ is ±0.3 dex (Tokovinin 2014), so the distribution of projected separations is indeed representative of the semimajor axis distribution. However, any sharp features of the latter, if they existed, would be washed out in the distribution of s owing to projections and random orbital phases. Conversely, any detail of the separation distribution is suspicious if it appears only in one 0.5 dex bin. Considering the projections, it makes sense to compute the smoothed separation distribution by using sliding bins, as in Figure 17.

The separation distributions in Figure 17 and Table 7 show an excess of pairs with separations below 100 au relative to the field. In the 9–90 au bin, the companion frequency in the field is 0.115 ± 0.007 and 0.110 ± 0.007 for early M- and solar-type stars, respectively. The companion frequency in USco in this bin exceeds that in the field by 1.75 ± 0.35 and 1.72 ± 0.33 times, respectively. The formal significance of

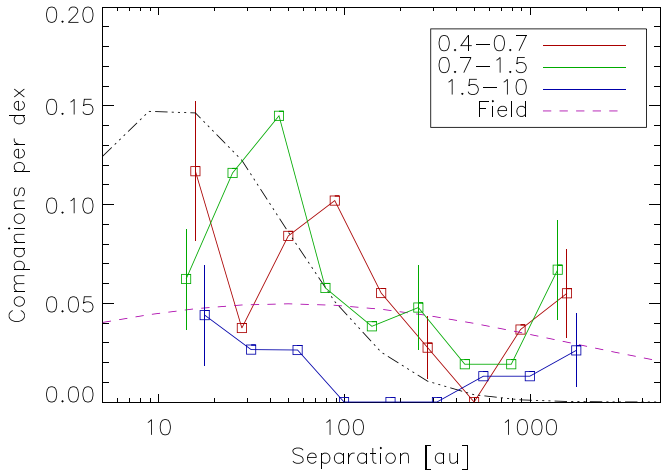

Figure 18. Same as Figure 17 but for binaries with $q > 0.7$. The dashed–dotted line is the lognormal distribution of multiperiodic binaries in USco found by Tokovinin & Briceño (2018) with arbitrary normalization.

both ratios, measured independently of each other, is $\sim 2.2\sigma$. In the full 2.5 dex separation range, the excess of early M- and solar-type binaries in USco over the field is 1.62 ± 0.22 and 1.39 ± 0.18, respectively. This excess therefore seems real, and with our significantly larger sample, it weighs importantly on growing evidence from previous studies, like that of Duchêne et al. (2018), based on smaller sets of stars. It is noteworthy that the frequency of companions does not increase with mass, contrary to the binary statistics in the field.

The dependence of the mass ratio distribution on separation means that the separation distribution also depends on the mass ratio. Concentration of binaries with large q at small separations is evident in Figure 15. When we compute the separation distribution only for binaries with $q > 0.7$, the dearth of pairs with separations of a few hundred au becomes more obvious (Figure 18). The excess of close and large-q binaries over similar solar-type pairs in the field is even stronger for stars less massive than $1.5\,\mathcal{M}_\odot$. As for the more massive binaries, they prefer small q and do not show any excess for $q > 0.7$. More strikingly, we note an underabundance of binaries with separations of $\sim$500 au in all three mass ranges. However, such binaries with even larger separations $s > 1000$ au are no longer underabundant. The mass ratio distribution at separations between $1''$ and $10''$ is modeled by $\gamma_{0.3} = -0.7 \pm 0.5$ and $f_{\rm twins} = 0$ (Table 6), indicative of a preference for low-q binaries and paucity of large-q pairs at these intermediate separations. The deficit of large-q binaries is further discussed in Section 6.

5.3. Clustering and Trapezia

To distinguish real wide binaries from chance projections of association members, we explored clustering of the USco members. For each primary star in the filtered sample, we computed the number of neighbors in the full (unfiltered) Luhman's sample within a set of 11 angular distances ρ from $10''$ to $1000''$, with a logarithmic step of 0.2 dex. These numbers $N(\rho)$ are plotted in the top panel of Figure 19. At $\rho > 200''$, the growth is approximately quadratic, as appropriate for a random distribution. At smaller separations, $N(\rho) \propto \rho^{0.7}$. The number of neighbors at close separations substantially exceeds the extrapolated number of chance

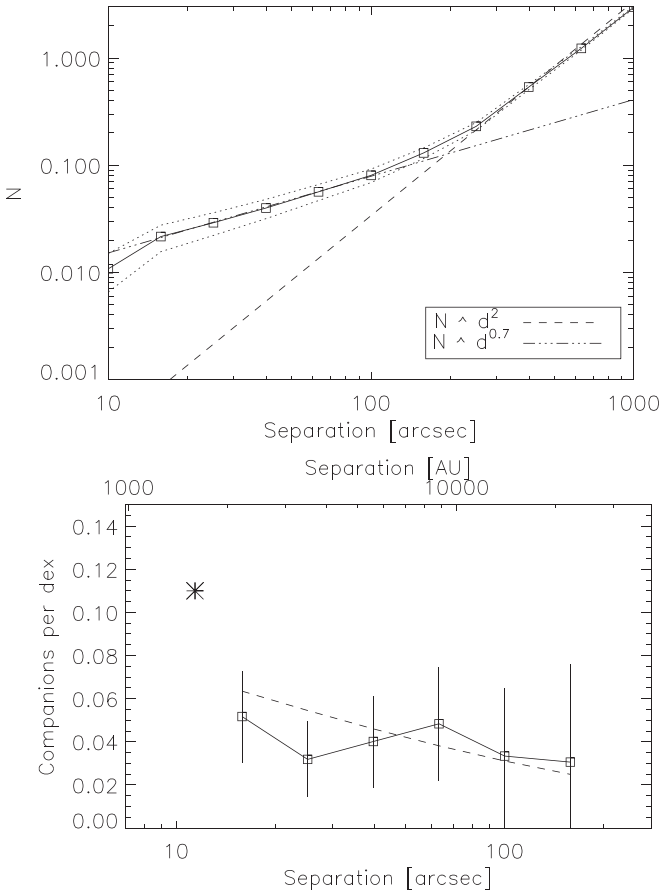

Figure 19. Clustering of the USco members. Top: average number of companions N per target within angular distance ρ (line and squares), with dotted lines showing the Poisson errors (they are not independent). The dashed and dashed–dotted lines are power laws at large and small separations, respectively. Bottom: distribution of projected separations after subtracting random asterisms (line and squares), with Poisson error bars. The dotted line is the lognormal distribution in the field for $q > 0.3$, and the large asterisk is the fraction of wide companions with $q > 0.3$ from Table 7.

alignments. Therefore, these pairs are mostly physical binaries rather than random pairs of association members.

In the bottom panel of Figure 19, the fraction of physical companions in each separation bin, scaled to the bin size of 1 dex, is plotted. The density of chance alignments of USco stars is estimated in the outermost ring, assuming that all of those pairs are random, scaled by the relative surface of the inner rings, and subtracted, leaving a number of physical (nonrandom) pairs. The companion frequency is approximately constant at ~ 0.04 dex^{-1} out to $\rho \sim 80''$ (10 kau); at larger separations, the increasing statistical errors prevent any conclusions. For comparison, the dashed line in Figure 19 shows the lognormal distribution of solar-type binaries with $q > 0.3$ in the field, and the asterisk is the frequency of wide $\sim$1600 au binaries with $q > 0.3$ for stars in the 0.4–1.5 $\mathcal{M}_\odot$ range, estimated above. The clustering analysis based on Luhman's sample does not restrict the range of mass ratios and is subject to the sample incompleteness. Therefore, the companion frequency plotted in Figure 19 is a lower limit. All we can say is that wide ($s > 10{,}000$ au) binaries in USco and the field have similar separation distributions.

Akter & Goodwin (2019) suggested using the distribution of the ratio r_{10} of the distances to the nearest and 10th-nearest

Table 8
Mini-clusters (Trapezia)

USn	ρ (arcsec)	θ (deg)	ΔG (mag)	ϖ (mas)	μ_α^* (mas yr^{-1})	μ_δ (mas yr^{-1})
US0123A	…	…	…	8.24 ± 0.10	−18.5	−28.1
US0123B	14.899	210.3	5.19	8.02 ± 0.11	−19.7	−27.4
US0123Ca	16.375	102.3	5.84	8.02 ± 0.09	−18.2	−27.0
US0123Cb	17.903	102.2	7.09	8.20 ± 0.14	−18.5	−27.9
US0133A	…	…	…	6.95 ± 0.05	−15.9	−23.6
US0133B	8.855	319.2	3.76	8.99 ± 0.22	−15.6	−22.2
US0133C	14.525	298.75	6.74	7.01 ± 0.16	−15.6	−21.8
US1394A	…	…	…	7.22 ± 0.10	−5.7	−27.6
US1394B	1.798	225.4	4.33	9.53 ± 0.56	−7.5	−25.4
US1394C	2.888	359.9	5.92	6.91 ± 0.71	−4.2	−27.5

neighbor to distinguish between physical binaries and chance projections in samples with nonuniform spatial distribution. We computed distances of 602 main targets of the filtered sample to the members of the full sample and derived the distribution of the resulting parameter r_{10}. It contains the expected signature of physical binaries with a frequency of ∼0.05. In other words, this method indicates that ∼30 wide pairs in Luhman's sample are physical binaries.

Clustering in USco was studied previously by Kraus & Hillenbrand (2008) using the list of association members available at that time. They found that the source density is uniform at spatial scales between 75″ and 1.°7. At larger scales, not probed here, the spatial distribution retains a memory of the primordial clustering, while separations below 75″ correspond to binary stars. We find the transition from binaries to random projections (intersection of the two lines in Figure 19) at ≈200″ (30 kau). After subtracting random projections of association members, the existence of binaries with separations beyond 10 kau is evidenced statistically.

A young stellar cluster is expected to retain some large-scale structure from its parental molecular cloud (Kraus & Hillenbrand 2008). Nonhierarchical groups of stars that formed close together (mini-clusters or trapezia) are dynamically unstable and disperse on a timescale of ∼100 crossing times; smaller groups disperse first. Indeed, all three compact nonhierarchical asterisms found at SOAR (Figure 8) turned out to contain only one physical pair each, the other stars being unrelated objects. On the other hand, we found three wider nonhierarchical groups of USco members around targets US0123, US0133, and US1394. For each group, Table 8 gives relative positions, magnitude differences, and astrometry from GDR2. The parallax of US0133B differs from the parallaxes of the other two neighboring stars by 2 mas, so this could be an association member seen in projection onto a 14.″5 binary A,C. As for the group US1394, the component B is measured at SOAR, while the fainter star C is below the SOAR detection limit (it is barely detectable in the average image). The component B could be a projection, considering its slightly different parallax and PM.

The group surrounding US0123 merits special attention. The parallaxes and PMs of its members are mutually consistent. The component B is identical to the target US0122, resolved at SOAR as a 0.″05 pair (Figure 7). The WDS lists another companion to this star (KOH 55 at 1.″58) that is not seen at SOAR and in GDR2 and hence is not considered here as real. The components Ca and Cb, both discovered in GDR2, apparently form a 1.″5 pair Ca,Cb. The group thus contains at least five stars structured as two pairs in the vicinity of the central star of 1.7 $\mathcal{M}_\odot$. Interestingly, there are no other USco members within 2′, according to GDR2, although a concentration of other targets in this area ($\alpha = 238.°82$, $\delta = -23.°37$) is visible in Figure 1.

If one of the separations in this group is shortened substantially by projection, this could be a hierarchical system, despite its configuration. If, on the other hand, this is a genuine trapezium, it could still survive disruption, at least in principle. A separation of 15″ corresponds to an orbital period of ∼70 kyr and a crossing time of the same order; the age of USco is at least 100× longer.

6. Discussion

Usually, the distributions of binary separations and mass ratios are analyzed separately (e.g., Duchêne & Kraus 2013), implicitly assuming that they are mutually independent. A more detailed examination of binary statistics in the field reveals that the mass ratio does depend on the separation, and vice versa (Moe & Di Stefano 2017); close pairs tend to have more equal components.

The discovery of the relative paucity of binaries with $q > 0.7$ at projected separations of $s \sim 500$ au (∼3.″5 at 140 pc), compared to both smaller and larger separations (Figure 18), appears to be a new result. This gap is present in three ranges of mass, strengthening its reality. Binaries with smaller mass ratios at these separations are not deficient, and the overall separation distribution in Figure 17 has only a minor (if any) depression around $s \sim 500$ au. We verified that this effect is unlikely to be produced by a bias against semi-resolved (blended) targets in our input sample (see Section 4.4).

This effect explains the apparent paradox found by Tokovinin & Briceño (2018), namely the unusually close separations of multiperiodic binaries in USco. They follow a lognormal distribution with a median of 11.6 au and a dispersion of 0.6 dex. Binaries qualify as multiperiodic if both components contribute substantially to the total light (hence a large q) and are an unresolved source in *Kepler* ($\rho < 4''$). Figure 18 shows that the narrow lognormal separation distribution of multiperiodic binaries found by Tokovinin & Briceño (2018) qualitatively fits the data at $s < 500$ au, before the minimum.

A relative paucity of binaries in USco with separations larger than 1″ and equal components compared to Taurus–Auriga was noted by Koehler et al. (2000) in their Section 5.3, but their conclusion was not statistically significant, owing to the small sample size (104 stars). This effect was noted again by Lafrenière et al. (2014). Meanwhile, the compilation of multiplicity surveys of young stars in Figure 12 of King et al. (2012) suggests that a similar effect may be present in other groups, most prominently in the ONC studied by Reipurth et al. (2007); see the lower panel of Figure 14.

If the narrow separation distribution found by Tokovinin & Briceño (2018) is extrapolated to small separations, it would imply an absence of very close (spectroscopic) pairs. This is unlikely, given that nine eclipsing binaries in USco are known (David et al. 2019). No large radial velocity (RV) surveys of USco have been made so far to probe this regime. Kuruwita et al. (2018) monitored RVs of 55 disk-bearing members of USco and estimated the frequency of spectroscopic binaries at $0.06^{+0.07}_{-0.02}$, like in the field and other star-forming regions (Duchêne & Kraus 2013). The presence of spectroscopic binaries in several northern associations and clusters (not including USco) has been probed by Kounkel et al. (2019) using RV measurements from APOGEE. They found that the frequency of close binaries with $a < 10$ au, detectable by their survey, is compatible with solar-type stars in the field and does not differ substantially between the studied regions. Interestingly, they discovered a deficit of double-lined (large-q) pairs among disk-bearing stars, like those surveyed by Kuruwita et al. (2018), that is recovered by the small-q single-lined systems with disks. It was also noted by RSC18 that multiperiodic stars in USco (large-q binaries) have a reduced incidence of disks. They speculated that binaries destroy their disks faster than single stars. However, the situation might be more complex, considering that many young low-q spectroscopic binaries do have disks (Kounkel et al. 2019).

Koehler et al. (2000) estimated the CSF in USco in the separation range from 0.″13 to 6″ as 0.35 ± 0.06, a factor of 1.6 ± 0.3 larger compared to the field. Most notably, their Figure 7 shows that the CSF increases with decreasing mass, contrary to the trend in the field. We confirm these findings, especially for binaries with $q > 0.7$. We find that the mild excess of binaries in USco compared to the field, 1.39 ± 0.18 for solar-type stars and 1.62 ± 0.22 for early M-type stars, is produced by pairs with $s < 100$ au and a large q; at wider separations, the binary frequency is similar or even lower than in the field.

Kraus et al. (2008) studied multiplicity in USco for a sample of 82 stars with masses from 0.3 to 1.7 $\mathcal{M}_\odot$ observed at the Keck telescope with a high angular resolution and a high contrast in the K band. Also using published data and seeing-limited imaging for 51 pairs, they derived a CSF of $0.35^{+0.05}_{-0.04}$ in the separation range of 6–435 au (1.9 dex), independent of the primary mass and only marginally (1.3 times) larger than the CSF of solar-type stars in the field, 0.27 (for all q). However, the small size of their sample precluded a more detailed characterization of the binary statistics. Kraus et al. (2008) also noted the paucity of binaries with masses in the 0.25–0.7 $\mathcal{M}_\odot$ range at $s > 200$ au. Figure 6 of Duchêne et al. (2018) shows that the excess of young binaries over the field is most prominent at separations $s < 100$ au; they found such an excess in the ONC from eight close pairs discovered by their survey.

Unfortunately, many multiplicity surveys of young stars do not specify detection limits in terms of mass ratio or do not estimate q at all, giving as an excuse uncertain isochrones and ages, variability, or infrared excess. The derived companion fractions are therefore difficult to compare between themselves or with the field. Moreover, previous multiplicity surveys (including those in USco) covered wide ranges of stellar masses because modest samples did not allow them to probe the dependence of multiplicity on mass.

Solar-type binaries in the field have a uniform distribution of mass ratios that does not depend on the period (Raghavan et al. 2010; Tokovinin 2014). Although Moe & Di Stefano (2017) found $\gamma_{0.3} \approx -0.5$ for the 25 pc sample, the best-fitting single power law in the full range $0 < q < 1$ is $\gamma \approx 0$. In contrast, the mass ratios of binaries in USco do depend on their separation for all masses. Pairs with $s \sim 10-20$ au have $\gamma_{0.3} \approx 1.5$ and a nonnegligible fraction of twins; $f(q)$ becomes nearly uniform only at larger separations. Also, the deficit of binaries with $q > 0.7$ and separations around 500 au noted in USco is not observed in the field. Finally, in USco, the companion fraction does not decrease with decreasing mass. These differences indicate that binary statistics is not universal and that star formation regions produce binary populations with varying properties. The same conclusion was reached by Duchêne et al. (2018) for the ONC and by King et al. (2012), who compared multiplicity in seven young groups, including USco. They noted an excess of close ($s < 100$ au) binaries in all young populations. These hard binaries are unlikely to be destroyed by dynamical interactions. Therefore, the multiple star formation (and, by extension, the star formation in general) is not universal.

7. Summary

The main results of our survey are as follows.

1. The sample of 614 members of USco more massive than 0.4 $\mathcal{M}_\odot$ from the list of L18 has been observed with a spatial resolution of 0.″05, expanding by an order of magnitude the previous multiplicity surveys of this region. We discovered 55 new pairs. Some of them are good candidates for future determination of orbits and masses.
2. New observations, published surveys, and *Gaia* DR2 astrometry are combined to produce the catalog of 250 physical binaries in USco with separations up to 20″. Limits of companion detection around each target are quantified.
3. We found that the mass ratio distribution $f(q)$ depends on the separation. The distribution at $q > 0.3$ is modeled by a truncated power law with index $\gamma_{0.3}$ and an additional fraction of twins with $q > 0.95$. For stars with masses between 0.4 and 1.5 $\mathcal{M}_\odot$, the power index changes from $\gamma_{0.3} = 1.5 \pm 0.6$ in the projected separation range 7–70 au, to $\gamma_{0.3} = 0.4 \pm 0.5$ in the intermediate (70–175 au) range, to $\gamma_{0.3} = -0.2 \pm 0.4$ in the 175–2800 au range. At the same time, the fraction of twins decreases from 0.15 ± 0.08 to zero.
4. The distribution of separations and the companion fraction are broadly compatible with those of solar-type stars in the field, with a mild excess of pairs at separations <100 au. However, unlike in the field, there is no dependence of the CSF on the stellar mass. In the

separation range from 9 to 2800 au, we measure CSF = 0.35 ± 0.04 for $q > 0.3$ and masses between 0.7 and 1.5 $\mathcal{M}_\odot$ and CSF = 0.33 ± 0.04 for masses from 0.4 to 0.7 $\mathcal{M}_\odot$. For comparison, solar- and early M-type stars in the field have a CSF of 0.110 and 0.115, respectively, in the same range of separations and q. In both mass ranges, the excess over the field is established with a statistical significance exceeding 2σ.

5. We discovered a deficit of binaries with $q > 0.7$ at intermediate separations from 200 to 500 au; such binaries are present at both smaller and larger separations. The deficit is seen for stars of all masses. It explains the unusually compact distribution of separations found by Tokovinin & Briceño (2018) for multiperiodic stars; those binaries with large q are mostly closer than 1″ owing to the deficit at larger separations. This effect, not present in the distribution of the field binaries, might be discernible in other groups of young stars.
6. The multiplicity statistics in USco differs from the field in several important aspects.

Our survey would have been impossible without the technical support provided by the SOAR telescope team and the CTIO engineers; we thank all those involved. We also appreciate the allocation of some engineering time for this survey by the SOAR director, J. Elias. The detector of HRCam was kindly loaned by N. Law. We thank the anonymous referee for helping us to improve the presentation and sharpen our conclusions.

This work used bibliographic references from the Astrophysics Data System maintained by SAO/NASA and the Washington Double Star Catalog maintained at USNO. We relied heavily on the data from the European Space Agency (ESA) mission *Gaia* (https://www.cosmos.esa.int/gaia), processed by the *Gaia* Data Processing and Analysis Consortium (DPAC; https://www.cosmos.esa.int/web/gaia/dpac/consortium). Funding for the DPAC has been provided by national institutions, in particular the institutions participating in the *Gaia* multilateral agreement.

Facility: SOAR.

Appendix
Comments on Individual Binaries

Some pairs listed in our binary catalog (Table 5) merit individual comments. The comments are assembled below in Table 9. Each binary is identified by its WDS-style code and the USn number.

Table 9
Notes on Individual Binaries

WDS	USn	Text of the Note
15322–2158	0	KOU 39 (0.″69, $\Delta K = 3.8$ mag) is not confirmed at SOAR; below detection limit of KOU05; ignored.
15360–2324	5	KSA 114AB (0.″055, $\Delta K = 3.0$ mag) is not resolved at SOAR; below our detection limit.
15415–2521	15	LAF 8 at 3.″7 is not seen at SOAR and by *Gaia*; ignored.
15481–2513	44	HDS 2226 has an orbit with a period of 31.2 yr.
15522–2141	84	The *Gaia* companion at 4″ is outside the SOAR field. A faint companion at 2.″6, 110° is assumed optical.
15527–2705	89	A triple system: A,B at 18.″2 (*Gaia*) and Aa,Ab at 0.″66 (SOAR).
15536-2520	97	SOAR does not confirm the 0.″1 occultation pair; only the 2″ binary BU 36AB is seen.
15539–2432	100	OCC 161 at 0.″1, discovered in 1932, is not confirmed at SOAR.
15553–2322	122	KOH 55 at 1.″5 is not confirmed, but a new 0.″05 pair is discovered. This is the secondary component to US0123, at 14.″9 and 5.2 mag brighter.
15558–2512	133	Trapezium with companions at 8.″9 and 14.″9. The 8.″9 pair with a slightly different parallax is ignored.
15580–3144	193	HNK 4 (0.″1, $\Delta K = 3.0$ mag) is tentatively resolved at SOAR well below the detection limit.
15592–2606	239	KSA 78AB is triple because the secondary, at 2.″9, is resolved as a 0.″07 pair B,C.
16000-2221	264	A new SOAR triple (A,B at 0.″30 and B,C at 0.″07). The 0.″025 pair KSA 122 is ignored; too close.
16001–2027	288	KOH 63 has a retrograde motion of 10° in one year; candidate for an orbit.
16022–2241	349	The pair LAF 94AC (0.″33, $\Delta K = 4.0$ mag) is unresolved at SOAR; below the contrast limit.
16030–2257	378	KSA 81 (1.″2, $\Delta J = 2.7$ mag) is unresolved at SOAR (contrast $\Delta I > 3.0$ mag) and by *Gaia*. The discovery measure appears to be below the claimed detection limit, hence we ignore this pair.
16034–1752	390	A new triple: Aa,Ab at 0.″1 (SOAR) and A, B = KSA 82 at 2.″5, measured by *Gaia* and SOAR.
16039–2032	413	KOH 70 has an orbit with $P = 52$ yr (Tokovinin & Briceño 2018).
16040–1751	417	The 2.″2 pair with $\Delta G = 4.3$ mag is measured by both *Gaia* and SOAR. Negative GDR2 parallax for B. The pair moved by 76 mas and is considered here as optical.
16044–2131	432	A star at 16.″2, 1.7 mag brighter, USco member, is found in GDR2, but not in the sample. Ignored.
16048–1749	447	Trapezium. The 2.″85 companion is physical, another at 3.″5 is optical, as well as two other fainter stars.
16048–1930	446	MET 69Aa,Ab at 0.″04 has two resolutions in the literature, unresolved at SOAR (too close?).
16054–1948	482	A massive quadruple; the orbits of BU 947AB and MCA 42CE (US0483), at 13.″7, are known.
16057–2150	501	LAF 104AC at 0.″13, $\Delta K = 2.0$ mag, is not confirmed by SOAR; closed down? Accepted as real.
16061–2336	521	RAS 25 (0.″1, $\Delta I = 3.3$ mag) is below SOAR detection limit. Owing to *Hipparcos* acceleration, considered real.
16070–2033	569	KSA 85BA (11.″8): B is a 0.″066 pair TOK 744CD; brighter than A=US0571.
16075–2546	613	A *Gaia* companion at 17″, 0.52 mag brighter; not in Luhman's sample; ignored.
16082–1909	651	KSA 127AB (0.″025) is below the SOAR limit; unresolved.
16084–1930	660	A *Gaia* pair at 13.″4; the secondary is US0663.
16087–2341	686	OCC 103 (0.″1 in 1930) is not confirmed at SOAR; considered spurious.
16087–2523	685	A new 0.″05 subsystem Aa,Ab in JNN 221 is detected in 2018.25 but unresolved (or marginally) in 2019.
16090–1900	708	HNK 6Aa,Ab (0.″18) is not confirmed by KOH2000, LAF14, and at SOAR; ignored here. In contrast, the wider 0.″96 pair KOU 55AB is resolved in 2018.56 and unresolved in 2019.2; variable?

Table 9
(Continued)

WDS	USn	Text of the Note
16093–1927	728	KOU 55 (0.″88) has a new subsystem Aa,Ab at 0.″09, $\Delta I = 3.6$ mag, below SOAR detection limit?
16104–1904	797	KOH 76AB (4.″6, 6.°5) is confirmed by GDR2 as physical, but the 4.″5 pair, KSA 133AE is optical because it moves too fast. GDR2 gives no parallax for E.
16104–2306	801	KOU 56AB with $\Delta K = 3.2$ mag is unresolved at SOAR but confirmed by LAF14. Another faint star, LAF 123AC at 3.″06, is ignored; likely optical.
16105–1913	816	KSA 93Aa,Ab with $\Delta K = 3.0$ mag is unresolved at SOAR but confirmed by LAF14. The companion B at 5.″8 is physical; this is a triple system.
16107–1917	820	Discordant photometry: $\Delta G = 3.19$ mag, $\Delta I = 4.0$ mag; variable?
16120-1907	907	KOH 78AB has a variable companion? $\Delta K \sim 0$ in 1999, $\Delta R = 3.4$ in 2015, $\Delta G = 3.5$ mag in 2015.5.
16120–1928	908	BU 120AB and CHR 146Aa,Ab is a known triple system.
16125–2332	934	A new triple. The companion at 1.″6 is assumed physical; it is too faint for *Gaia*.
16127–1859	945	GHE 20Aa,Ab (0.″12) is securely unresolved at SOAR, despite $\Delta K = 1.5$ mag and several measures. This is a companion to US0947, at 19″. Considered as independent in the statistics.
16128–1801	957	The 3.″2 *Gaia* pair is below the SOAR detection limit (too wide and faint).
16130–2245	964	Trapezium asterism. The 5.″4 companion is physical; the 3.″6 one is optical.
16133–2922	985	Close on the sky is KOH 70 (EPIC 20252205) with a $P = 52$ yr orbit, missed in Luhman's sample.
16140–2815	1019	Classical binary RST 1883; orbit calculation is possible.
16156–2622	1107	*Gaia* measured $\Delta G = -0.05$ mag. Also measured at SOAR. Set $\Delta G = 0.05$ mag.
16160–2325	1123	The 2.″5 SOAR pair with $\Delta I = 3.3$ mag is not present in *Gaia* and ignored.
16164–2459	1146	KOU 59 is unresolved at SOAR, 0.″94, $\Delta K = 4.4$ mag; below the detection limit.
16188–2328	1248	The *Gaia* companion at 8.″5, $\Delta G = -0.23$ mag, is accepted with $\Delta G = 0.23$.
16193–2329	1273	Triple asterism in SOAR and *Gaia*. The 0.″9 pair A,B is physical; the 1.″9 one is optical.
16205-2007	1327	B 1808AB, discovered at 0.″2 in 1929, is now at 0.″07; opening. The outer pair SHJ 226AC is at 12.″6.
16209–2254	1345	The secondary at 9.″9 is US1344.
16212–2536	1351	The 3.1 mas interferometric subsystem NOR 1Aa,Ab is ignored; outside the surveyed range.
16212–2342	1353	SOAR and *Gaia* measure the 1.″6 pair at different positions, discordant parallax, optical.
16222–1953	1394	*Gaia* trapezium: A,B at 1.″8, A,C at 2.″89. A,B is confirmed at SOAR; A,C is barely seen.
16239–3312	1443	The companion at 6.″2 is US1444.
16263–2233	1486	The secondary at 10.″5 is US1487.
16298–2152	1531	MET 77AB (3.″1, $\Delta K = 5.8$ mag) is fixed in 2002–2012; physical. Not seen by *Gaia*, barely by SOAR.
16320–2530	1551	The secondary at 14.″2 (BOV 58) is US1553.
16336–1833	1562	The faint *Gaia* companion at 3.″3 is at the edge of the SOAR image.
16359–2813	1578	The 21 mas pair RIZ 18 is below the SOAR resolution limit.

ORCID iDs

Andrei Tokovinin https://orcid.org/0000-0002-2084-0782

References

Akter, S., & Goodwin, S. P. 2019, MNRAS, 488, 3446
Bate, M. R. 2014, MNRAS, 419, 3115
Bouy, H., Martín, E. L., Brandner, W., et al. 2006, A&A, 451, 177
Brandeker, A., & Cataldi, G. 2019, A&A, 621, A86
Briceño, C., & Tokovinin, A. 2017, AJ, 154, 195
Damiani, F., Prisinzano, L., Pilliateri, I., et al. 2019, A&A, 623, 112
David, T. J., Hillenbrand, L. A., Gillen, E. F., et al. 2019, ApJ, 872, 161
Duchêne, G., & Kraus, A. 2013, ARA&A, 51, 269
Duchêne, G., Lacour, S., Moraux, E., et al. 2018, MNRAS, 478, 1825
Esplin, T. L., Luhman, K. L., Miler, E. B., et al. 2018, AJ, 156, 75, (E18)
Gaia Collaboration, Brown, A. G. A., Vallenari, A., et al. 2018, A&A, 595, A2
Hinkley, S., Kraus, A. L., Ireland, M. J., et al. 2015, ApJ, 806L, 9
Janson, M., Lafrenière, D., Jayawardhana, R., et al. 2013, ApJ, 773, 170
King, R. R., Goodwin, S. P., Parker, R. J., & Patience, J. 2012, MNRAS, 427, 2036
Koehler, R., Kunkel, M., Leinert, C., & Zinnecker, H. 2000, A&A, 356, 541
Kounkel, M., Covey, K., Moe, M., et al. 2019, AJ, 157, 196
Kouwenhoven, M. B. N., Brown, A. G. A., Zinnecker, H., et al. 2005, A&A, 430, 137
Kraus, A. L., & Hillenbrand, L. A. 2008, ApJL, 686, L111
Kraus, A. L., & Hillenbrand, L. A. 2012, ApJ, 757, 141
Kraus, A. L., Ireland, M. J., Martinache, F., & Lloyd, J. P. 2008, ApJ, 679, 762
Kroupa, P. 2001, MNRAS, 322, 231
Kroupa, P., & Petr-Gotzens, M. G. 2011, A&A, 529, 92
Kuruwita, R. L., Ireland, M., Rizzuto, A., et al. 2018, MNRAS, 480, 5099
Lafrenière, D., Jayawardhana, R., van Kerkwijk, M. H., et al. 2014, ApJ, 785, 47
Luhman, K. 2018, AJ, 156, 271
Luhman, K. L., Hermann, K. A., Mamajek, E. E., et al. 2018, AJ, 156, 76, (L18)
Mason, B. D., Wycoff, G. L., Hartkopf, W. I., Douglass, G. G., & Worley, C. E. 2001, AJ, 122, 3466, (WDS)
Metchev, S. A., & Hillenbrand, L. A. 2009, ApJS, 181, 62
Moe, M., & Di Stefano, R. 2017, ApJS, 230, 15
Parker, R. J., & Meyer, M. 2014, MNRAS, 442, 3722
Press, W. H., Flannery, B. P., Teukolsky, S. A., & Vetterling, W. H. 1986, Numerical Recipes. The Art of Scientific Computing. (Cambridge: Cambridge Univ. Press)
Raghavan, D., McAlister, H. A., Henry, T. J., et al. 2010, ApJS, 190, 1
Rebull, L. M., Stauffer, J. R., Cody, A. M., et al. 2018, AJ, 155, 196, (RSC18)
Reipurth, B., Guimarães, M. M., Conneley, M., & Mally, J. 2007, AJ, 134, 2272
Reipurth, Bo., Clarke, C. J., Boss, A. P., et al. 2014, in Protostars and Planets VI, ed. H. Beuther et al. (Tucson: Univ. of Arizona Press), 267
Shatsky, N., & Tokovinin, A. 2002, A&A, 382, 92
Tang, J., Bressan, A., Rosenfield, P., et al. 2014, MNRAS, 445, 4287
Tokovinin, A. 2014, AJ, 147, 87
Tokovinin, A. 2018, PASP, 130, 5002
Tokovinin, A., & Briceño, C. 2018, AJ, 156, 138
Tokovinin, A., Mason, B. D., & Hartkopf, W. I. 2010, AJ, 139, 743
Tokovinin, A., Mason, B. D., Hartkopf, W. I., et al. 2018, AJ, 155, 235
Tokovinin, A., Mason, B. D., Mendez, R. A., et al. 2019, AJ, 158, 48
Winters, J. G., Henry, T. J., Wei-Chun, J., et al. 2019, AJ, 157, 216
Wright, N. J., & Mamajek, E. E. 2018, MNRAS, 476, 381